$\gamma\gamma$ Physics at Linear Colliders

Conveners: P. Aurenche, A. Finch, M. Greco, D.J. Miller

Working group: M. Baillargeon, G. Bélanger, J. Blümlein, F. Boudjema, M. Cacciari, D. Choudhury, A. Corsetti, V. Del Duca, R. Engel, M. Fontannaz, I.F. Ginzburg, R.M. Godbole, J.-Ph. Guillet, G. Jikia, M. Krämer, M. Krawczyk, E. Laenen, G. Pancheri, J. Ranft, S. Riemersma, D.J. Schulte, T. Sjöstrand, A. Vogt

1 Introduction

As it is well known, there are several ways to generate photon-photon collisions at linear e^+e^- colliders. Bremsstrahlung and/or beamstrahlung photons radiated by the incoming electrons will interact with a center of mass energy which is only a small fraction of the available e^+e^- energy. These collisions are a nuisance for studies in electroweak interactions as they reduce the available e^+e^- luminosity at a given energy and generate an important hadronic background. Much work is going on to reduce this component. However it will be seen that this mechanism can be used to understand the deep structure of the photon. On the other hand, dedicated photon linear colliders can be constructed using backward Compton scattering of a beam electron on a laser photon, which will yield a photon-photon energy similar to the e^+e^- energy with a high luminosity: such colliders are invaluable for the study of multiple gauge boson couplings and will also allow studies of the hadronic structure of the photon at short distances never reached before. In this chapter we deal, partially, with all these aspects. Bremsstrahlung and/or beamstrahlung collisions will be discussed from the point of view of its relevance for QCD studies while for the photon linear colliders we discuss both its implications for QCD and electroweak theories.

Compared to previous reports [1] it will be seen that considerable progress has been achieved concerning both soft and hard (hadronic) physics studies: this is the result of the recent LEP2 [2, 3] workshop as well as the recent experimental studies at HERA [4]-[6]. More progress is obviously expected in the near future so that one should have a quantitative description of hadronic phenomena and therefore a good control of the "background" to "interesting" or new physics. Roughly speaking, making use of proton-antiproton studies at the FERMILAB collider and photon-proton studies at HERA one should be able, based on a loose concept of factorization, to predict reliably photon-photon physics at high energies. LEP2 results will provide a stringent test of these ideas. Concerning electroweak studies, during this workshop, radiative corrections to W pair production have been calculated as required for future precision studies and detailed signature of anomalous gauge boson couplings are being proposed, which are more stringent than those in the e^+e^- channel.

The report opens with Ginzburg overall perspective of the physics possibilities of photon linear colliders: in QCD the extended kinematical range available will make it possible to probe the so-called BFKL or Lipatov Pomeron which is now under discussion in connection with recent Hera data. The relevance of a linear collider for Higgs discovery in the range 80 GeV to $2M_Z$ is stressed as well as its importance as a W boson factory and corresponding precision tests. A fundamantal theoretical problem still to be solved is that of gauge theories with unstable particles.

As a prerequisite to more detailed physics studies, Schulte gives a status report of the beamstrahlung spectrum and its associated bakground at TESLA before discussing the possible configuration and features of a linear $\gamma\gamma$ collider.

The study of the deep-inelastic structure of the photon is discussed next: the basic

process is $\gamma^*\gamma$ scattering, the virtual photon being necessarily emitted by bremsstrahlung. The main limitations arise from the detector configuration: if no $e^{\pm}$ detector is installed inside the shielding mask the available kinematical range is drastically reduced: $Q^2 > 10^3$ GeV^2 and $x > 10^{-2}$ leaving no overlap with the LEP2 results. To explore the full range of $x > 3.10^{-4}$ and Q^2 values up to 10^5 GeV^2 it will be necessary to use $e\gamma$ colliders . At such small x values the behavior of the photon structure function may not be controlled by the Dokshitser-Gribov-Lipatov-Altarelli-Parisi evolution equations and it may be necessary to resum the large $\ln x$ factors: the case of the gluon distribution is analysed below.

Turning to quasi real photon collisions new tools have been developped and event generators now exist (PYTHIA [7], PHOJET [8]) which take into account both soft and hard physics and which should be adequate up to the highest possible energies available for linear colliders. Detailed studies are going on to fine-tune these generators to all available photon initiated collisions (TRISTAN, LEP2, HERA) and compare their predictions. Particularly interesting are the possibilities to elucidate the nature of the perturbative Pomeron (semi-hard regime) in relation to rapidity gap events: $\gamma\gamma$ collisions have two avantages over hadron induced collisions: a) the variable $\gamma\gamma$ initial energy makes it possible to factorize the parton dynamics from the effect of parton-parton luminosities; b) choosing one initial photon to be virtual reduces the "underlying" event contribution which tends to fill the rapidity gaps in hadronic reactions. In the hard perturbative regime jet production can be used to probe the gluon content of the photon and thus complement the structure function studies which are essentially constraining the quark content.

Several aspects of heavy flavor production are examined both in $\gamma\gamma$ and $\gamma^*\gamma$ collisions in the next-to-leading order approximation of QCD. Inclusive rates as well as correlations are discussed. The production rate of charm is very large. Heavy flavor production offers the unique feature of separating a direct "component" unambiguously predicted in perturbative QCD from a "resolved" component sensitive to the gluon content of the photon: both component can be compared separatly to experimental data.

Of course, a e^+e^- collider is not going to be built only to further probe QCD at very short distances! The main aim is to discover the mechanism of symmetry breaking and understand the dynamics of electro-weak gauge boson interactions. Considerable progress has been made with the complete one-loop calculation (both real and virtual diagrams included) of the process $\gamma\gamma \to W^+W^-$ in the Standard Model. This is discussed below.

The study of anomalous $WW\gamma$ couplings has witnessed important developments: taking into account the $W \to f\bar{f}$ decay, interference between the anomalous W_LW_L channel and the standard W_TW_T channel is possible and found to be large so that an enhanced sensitivity to anomalous $WW\gamma$ couplings is obtained. Using, furthermore, a multivariable maximum likelihood fit a considerable improvement on the determination of the anomalous couplings is possible. This requires however $\gamma\gamma$ energies of the order of 800 GeV. The study of the process $\gamma\gamma \to W^+W^-Z$ shows that WWZ couplings can also be probed at $\gamma\gamma$ energies above 1 TeV. These results call for more detailed studies.

Finally, a case is made for a low energy (10 GeV) linear $\gamma\gamma$ collider in order to probe the light Higgs sector, not presently excluded by LEP data, in the Two Higgs Doublet

Model.

References

[1] e^+e^- Collisions at 500 GeV: The Physics Potential, P.M. Zerwas ed., DESY 93-123C; Proceedings of the Workshop on Physics and Experiments with Linear e^+e^- Colliders, Waikaloa, Hawaii, April 1993, eds. F.A. Harris et al.

[2] $\gamma\gamma$ generators, L. Lönnblad and M. Seymour convenors, in *Physics at LEP2*, CERN Yellow report, CERN 96-01, G. Altarelli, T. Sjöstrand, F. Zwirner eds.

[3] $\gamma\gamma$ physics, P. Aurenche and G.A. Schuler convenors, in *Physics at LEP2*, CERN Yellow report, CERN 96-01, G. Altarelli, T. Sjöstrand, F. Zwirner eds.

[4] Proceedings of the Workshop on Two-Photon Physics at LEP and HERA, Lund, May 1994, G. Jarlskog and L. Jönsson *eds.* (Lund Univ., 1994).

[5] 10th Workshop on Photon-Photon Collisions (PHOTON'95), Sheffield, U.K, April 1995, B. Cartwright, D.J. Miller and V.A. Khoze *eds.*

[6] Workshop on Deep Inelastic Scattering and QCD, Paris, April 1995, J.F. Laporte and Y. Sirois *eds.*

[7] G. A. Schuler and T. Sjöstrand, Nucl. Phys. B407 (1993) 539; $\gamma\gamma$ and γp events at high energies, CERN-TH.7193/94, presented at the Workshop on Two-Photon Physics, Paris, 1994

[8] R. Engel, Z. Phys. C66 (1995) 203; R. Engel and J. Ranft, Hadronic photon-photon collisions at high energies, ENSLAPP-A-540/95 (hep-ph/9509373)

2 Key points of a physics program at photon colliders

Ilya F. Ginzburg

Institute of Mathematics, Novosibirsk. Russia

2.1 Basic points

Most of future e^+e^- linear colliders (LC) will be simultaneously photon colliders (PLC), *i.e.* $e\gamma$ or $\gamma\gamma$ colliders [1]. Modern studies show that one can expect the following features for PLC[1] (below we use the notation: E – initial electron energy, E_γ – photon energy, $E_{\gamma\gamma}$ or $E_{e\gamma}$ – c.m. energy of the photon–photon or electron–photon system):

- characteristic photon energy[2]: $E_\gamma \approx 0.8E$;
- mean energy spread: $< \Delta E_{\gamma\gamma}/E_{\gamma\gamma} > \approx 0.1$ (*monochromatic variant*);
- polarized photons with mean helicity $\lambda \approx 0.95$;
- measurements at small angles limited by difficulties of design only. Therefore, it is useful to add to the wide angle detector (which will be common for all modes of LC) a small angle detector for the PLC modes;
- expected annual luminosity: $\mathcal{L} \approx 10 \div 20$ fb^{-1} in the *monochromatic variant*. (It is $\sim 10\%$ of the geometrical luminosity $\mathcal{L}_g$. One can make $\mathcal{L}_g$ higher than the luminosisty for the basic e^+e^- LC. In particular for the TESLA project, one can obtain $\mathcal{L}_g \approx 10\ \mathcal{L}_{basic}$ [6].);
- in each case, possible *non-monochromatic variant* with $\gamma\gamma$ luminosity$\sim$ 5times higher with wide energy spectrum (and with almost the same high energy part of spectrum as in the monochromatic variant). The additional, softer photons are almost unpolarized in this case;
- in principle, possible *super-monochromatic variant* with $E_\gamma \approx 0.95E$; $< \Delta E_{\gamma\gamma}/E_{\gamma\gamma} > \approx 0.015 \div 0.02$ but with $\mathcal{L}$ about $10 \div 20$ times less;
- the monitoring of differential luminosity is necessary.

When the PLC is based on the e^-e^- collisions, the deflection of electrons after conversion is unnecessary[3]. Indeed, we do not expect any specific processes in the e^-e^- collisions (if such exotic processes exist, they should be studied without conversion). Most of the "parasitic" processes (from e^-e^-) with the production of some final state F are $\gamma^*\gamma^* \to F$ and $\gamma^*\gamma \to F$. The effect of these (almost real) virtual photons shows up entirely in the

[1] *The conversion region is an $e\gamma$ and a $\gamma\gamma$ collider with a small c.m. energy about 1 MeV, but with a huge luminosity $10^6 \div 10^8$ fb^{-1} per year.* It gives the possiblity to search for very light particles [4, 5].

[2] The free electron laser with the variable frequency seems to be useful to fix this relation at the initial electron energy variation.

[3] For the very dense electron beams this fact was established by Balakin (in this case these electrons are bent by strong electromagnetic field of opposite bunch).

measured photon luminosity spectrum. These virtual photons give a small deviation in the soft part of this spectrum. The highly virtual photons are accompanied by the (observable) electrons, scattered at large enough angle. Their flux is small. The specific $e\gamma$ processes like $e\gamma \to W\nu$, $e\gamma \to eWW, \cdots$ are known in advance. They can be studied simultaneously with the $\gamma\gamma$ processes owing to the specific signature.

Below I present only the key points of a physics program. I shall try not to repeat the problems, considered in other reports here. My list of references is very incomplete.

I will call the photon collider with the c.m. energy in the range 80–180 GeV PLC1. It can be the first stage of an entire linear collider project.

2.2 Hadron Physics and QCD

Hadron physics and QCD are the traditional fields for the $\gamma\gamma$ collisions. The $\gamma\gamma$ experiments provide new type of collisions and with the simplest quark structure of the pointlike initial state. The PLC will extend these studies to new regions. The results from PLC together with those from the Tevatron and HERA, will produce the entire set of data related to a factorized (in the old Regge sense) set of processes. In this respect, HERA gets a new importance of a bridge between PLC and Tevatron/LHC.

1) **Total cross section $\sigma(\gamma\gamma \to hadrons)$ and diffraction like processes in soft region**. The expected values are: $\sigma^{tot} \equiv \sigma_{\gamma\gamma\to hadrons} \sim 0.3\ \mu b$ in the SLC energy region, and $\sigma^{tot} \sim 0.5 \div 1\ \mu b$ at $E_{\gamma\gamma} \sim 2$ TeV [8]. Besides, $\sigma(\gamma\gamma \to \rho^0\rho^0) \sim 0.1\sigma^{tot}$ (see [9]). It is important to study the energy dependence of this cross section (together with the Q^2 dependence — in γe collisions). Its comparison with $\sigma_{pp}(\sigma_{p\bar{p}})$ and $\sigma_{\gamma p}$ will allow us to understand the nature of the hadron cross sections growth with energy. The crucial problem is to test the possible factorization of these cross sections (this factorization is assumed in ref. [8]). How can we measure this cross section?

2) **The semihard processes** are those, for which the characteristic value of transverse momentum is small in comparison with total energy but large in comparison with the strong interaction scale $\mu \sim 300$ MeV : $s \gg p_\perp^2 \gg \mu^2$. We consider here the diffraction like processes, including small angle jet production with rapidity gap. These phenomena give us information about the perturbative Pomeron and Odderon, mechanisms of shadowing in pQCD, etc. In this region, a new parameter appears in the pQCD series, $\alpha_s(p_\perp^2)ln(s/p_\perp^2) \approx \alpha_s(p_\perp^2)\eta$ or $\alpha_s(Q^2)ln(1/x)$, that becomes large while s increases. Therefore, the entire pQCD series should be taken into account, and studies here provide opportunity to test the inner structure of pQCD in all orders. Due to the simple pointlike nature of photons, the nontrivial results in pQCD could be obtained almost without model assumptions. Unfortunately, the influence of the hadronlike component of the photon is expected to be relatively small at large enough $p_\perp$ only. For example, for the diffraction like processes it is expected to be at $p_\perp > 7$ GeV [10].

The processes $\gamma\gamma \to \rho^0 X$, $\gamma\gamma \to \gamma X$, $\gamma\gamma \to \rho^0\phi$ with rapidity gap are described

by pure Pomeron exchange. They present the best opportunity to study the Pomeron. The processes $\gamma\gamma \to \pi^0 X$, $\gamma\gamma \to \pi^0 a_2$ with rapidity gap are described only by Odderon exchange. They present a unique opportunity for Odderon studies. This is in contrast with the fact that the Pomeron and the Odderon have identical status in pQCD. The cross sections of some processes, integrated over the range of $p_\perp > 7$ GeV[4] and with large enough rapidity gap, are estimated from below as [11, 12]:

$$\sigma_{\gamma\gamma \to \rho^0 X} \gtrsim 1\,pb, \quad \sigma_{\gamma\gamma \to \gamma X} \gtrsim 0.2\,pb, \quad \sigma_{\gamma\gamma \to \pi^0 X} \gtrsim 0.4\,pb$$

The first two quantities should be multiplied by the growing BFKL factor (see[13, 14]). Where is the corresponding boundary for the jet production with a rapidity gap? Where are the real bounds for the description of $s/p_\perp^2$ dependence with perturbative Pomeron or Odderon (both from below in $p_\perp$ and from above in $s/p_\perp^2$)?

2.3 Higgs Boson (Higgs) Physics

1) **The discovery of the Higgs**. The PLC1 seems to be the best machine for the discovery of Higgs with mass in the 80–180 GeV interval [15]. The process $\gamma\gamma \to H \to b\bar{b}$ with QED background $\gamma\gamma \to b\bar{b}$ was considered in [16, 17, 18]. In the monochromatic variant of PLC with zero total initial photon pair helicity, one can observe Higgs with mass $80 < M_H < 140$ GeV, based on a total luminosity about 3 fb^{-1}.
The mass interval 140 GeV $< M_H < 2M_Z$ is difficult for the Higgs discovery. The decay $H \to WW$ dominates here, but the WW production cross section via Higgs is less than that without this intermediate state. It was noted in ref. [19], that the total width of such a Higgs will be high enough to resolve details of WW spectrum within this width interval. Besides, the amplitude of the $\gamma\gamma \to H \to WW$ process is complex with a phase which varies rapidly: $\mathcal{M} \propto \Gamma(\gamma\gamma \to H)(s - M_H^2 + i\Gamma_H M_H)^{-1}\Gamma(H \to WW)$. Therefore, the interference of this amplitude with that for the QED process $\gamma\gamma \to W^+W^-$ is high. Ref. [19] shows the spectacular curves for 180 GeV $< M_H <$ 400 GeV[5]. Special simulation work is necessary to understand, what requirements are imposed on either PLC (monochromatization degree) or detector (accuracy of W decay products momenta measurements), to see the Higgs in the widest mass interval.

2) At the PLC only, one can measure the **Higgs two photon width**. This width is the counter for SM particles heavier than Higgs.

3) The investigation of the **Higgs coupling with the matter** is necessary to obtain whether the observed particle is actually a Higgs of the Standard Model (SM) or something else.

If $M_H < 150$ GeV, one could try to study the Higgs decay into $\tau\bar{\tau}$ or $c\bar{c}$ with SM branching ratios $\sim$ 0.06 or 0.04 (cf.[18]). These opportunities need for new work on simulation.

[4]It corresponds to the production angle above 70-100 mrad at PLC1.

[5]The amplitude of this interference is higher at lower s, since W's from Higgs decay are mainly longitudinal and the fraction of longitudinal W's from $\gamma\gamma \to W^+W^-$ process decreases with s.

If $M_H > 2M_Z$, one can compare Higgs coupling with Z and W (by comparison of Higgs production via reaction $\gamma\gamma \to H \to ZZ$ and via interference in $\gamma\gamma \to W^+W^-$ reaction).

If $M_H \sim 2M_t$, the interference between the QED process $\gamma\gamma \to t\bar{t}$ and resonant one $\gamma\gamma \to H \to t\bar{t}$ can be used to see the value of the Higgs coupling with the t-quark [20].

3) **The anomalous interactions of Higgs**. The SM Higgs with $M > 500$ GeV will be invisible in $\gamma\gamma$ collision. Therefore, any Higgs signal at a PLC in this region manifests the existence of either some heavier SM particles or nonstandard interactions of Higgs, having the scale about a few TeV [21, 36].

2.4 Gauge boson physics

The sketch of the **main processes with W and Z production** at PLC within the SM is given in refs. [22, 23]. The scale of these phenomena at PLC is the cross section of the $\gamma\gamma \to W^+W^-$ process at high enough energies $\sigma_W = 8\pi\alpha^2/M_W^2 \approx 81$ pb. Besides, in this limit we have $\sigma_{e\gamma\to W\nu} = \sigma_W/8\sin^2\Theta_W \approx 43$ pb. These very processes determines PLC as **W factory** with $10^6 \div 10^7$ W's per year.

The processes $e\gamma \to W\nu$ and $\gamma\gamma \to W^+W^-$ with their dependence on helicities of photon λ_γ and electron λ_e were considered in ref. [24]. The angular distribution of produced W's for both processes is more favorable for W recording than that in process $e^+e^- \to W^+W^-$. The $e\gamma$ cross sections at $E_{e\gamma} < 200$ GeV and the $\gamma\gamma$ cross sections at $E_{e\gamma} < 300$ GeV vary strongly with a variation of photon helicities. This polarization dependence disappears at higher energies.

Besides, the process $e\gamma \to W\nu$ is switched on or off entirely with variation of electron helicity ($\sigma_{e\gamma\to W\nu} = (1-2\lambda_e)(\sigma + \lambda_\gamma\tau)$). This means, that this process is very sensitive to an admixture of right–handed currents in W coupling with matter. On the other hand, this process can be used for testing initial electrons polarizations.

When the energy increases, the cross sections of a number of higher–order processes become large enough. The catalogue of such processes of third order in the SM is given in ref. [25]. Among the processes of highest interest is the process $e\gamma \to eW^+W^-$ with high cross section (25 pb at $\sqrt{s} \sim 2$ TeV). The difference of cross sections with opposite electron helicities (~ 5 pb) is proportional to the amplitude of the $\gamma Z \to WW$ subprocess (axial current contribution). Besides, a large enough fraction of cross section with unpolarized electrons occurs in the region of electron transverse momenta 50–150 GeV, which is very sensitive to the γZWW interaction [26].

In the processes with four gauge bosons in the final state (4-th order processes) we can see subprocesses with heavy gauge boson scattering. The SM cross sections for the processes $\gamma\gamma \to WWWW$ and $\gamma\gamma \to WWZZ$ are $\sim 0.3 \div 0.1$ pb [27]. The cross section of the process $e\gamma \to eWWZ$ is of the same order of value: $(\alpha/\pi)^2 \ln(s/m_e^2) \cdot \ln^2(s/4M_W^2)\sigma_{\gamma\gamma W^+W^-}$.

Some process of fifth and sixth order will be observable at high enough energies, for

example, $e\gamma \to e^+e^- eWW$, $e\gamma \to e^+e^- \nu WZ$, $\gamma\gamma \to e^+e^- \mu\bar{\mu}WW$, etc.

Problems in the gauge boson physics

1) **The incorporation of the W width and the problem of quantization**. To describe gauge boson production with real final states of the W decay, one should use the W propagator near its physical pole. To avoid divergence, it is necessary to insert in this propagator the W width Γ_W, for example, $(k^2 - M_W^2 - i\varepsilon)^{-1} \Rightarrow (k^2 - M_W^2 - iM\Gamma_W)^{-1}$. This simple change violates gauge invariance [28] and unitarity. It results in inaccuracy $\sim (1 \div 3)\Gamma/M$. The more likely recipes should eliminate the above violations. However, this requirement gives no unambiguous recipe. One can expect that the ambiguity of the result when using the different recipes, both unitary and gauge invariant, without genuine theory will be $\sim \alpha\Gamma/M$ ($\sim 10^{-3}$ or larger), i.e. the accuracy of such recipes seems to be deficient for the description of the data. Therefore, the well–known fundamental problem of quantum field theory becomes of practical importance here (see e.g. [29]):

It is necessary to construct a genuine theory of unstable gauge bosons.

2) The underlying interactions could manifest itself as the deviations from the SM in some **anomalous interactions of gauge bosons**. These anomalies are described by effective Lagrangians. The standard approach is to consider here operators of lower dimension – 4 and 6 (e.g. an anomalous magnetic moment, quadruple moment, etc.). These effects increase with energy, the larger energy is the better for their detection. Some results have been obtained for the e^+e^-500 LC (including PLC) [31, 32].

Usually the joined effect of all these anomalies is studied for some small set of processes ($e^+e^- \to WW$,...). The different processes (and different kinematical regions for one process) are sensitive in different manner to various possible anomalous gauge boson interactions. The PLC with their large set of observable processes provide opportunity to study various anomalies almost separately in the different processes. Special work is necessary to present detail program in this field.

3) One can measure the **elements of the Cabibbo–Kobayashi–Maskawa mixing matrix** on the mass shell of W. Their comparison with those obtained in the past and present experiments (far from W mass shell) can give an idea about their dependence on W boson virtuality.

4) The possibility of **strong interactions in the Higgs sector** seems to be a very probable one at $\sqrt{s} \gtrsim 1$ TeV. It could manifest itself at PLC as some resonances in the gauge boson systems, unusual energy dependence, multiple W production, etc. Its first signals could be obtained in the production of longitudinal W's and Z's. (For more details, see a number of papers, e.g., [33]). The SM cross section $\gamma\gamma \to Z_LZ_L$ is small [34]. However, experience in pion physics permits us to expect here large effects due to some heavy states (like ω in the t-channel for $\gamma\gamma \to \pi\pi$).

At large enough energies, one can expect to see the strong interaction of transverse W's driven by the strong Higgs self–interaction. Where does this energy region begin?

2.5 New Physics

Two opportunities are considered, when we speak about New Physics effects — the discovery of **new particles** and **new nonstandard interactions** of known particles.

PLC provide the best place to discover many new particles — in comparison with other colliders, having similar energy. The reasons for this statement are (see in more detail ref. [35]):

1) The signal to background ratio at PLC is often much better than that at hadron colliders.

2) The photons are "democratic" respective to all charged particles. Therefore, the analyses of new particles production have no additional ambiguities due to production mechanism at PLC (which exists in collisions with hadrons).

3) The (electrodynamic) cross sections of charged particles production at $\gamma\gamma$ PLC are larger than those at e^+e^- LC. Even if PLC luminosity is 5 times less than that for basic e^+e^- LC (standard monochromatic variant), the number of produced pairs at e^+e^- collider is no more than that at $\gamma\gamma$ collider. Besides, this production in $\gamma\gamma$ collision decreases with energy slower than that in e^+e^- collision. Therefore, one can study new particles relatively far from threshold with a good enough rate. In this region, the decay products of these particles overlapp weakly, and their detailed study becomes more feasible.

4) The $\gamma\gamma$ collisions often produce pairs of identical particles with identical decays (e.g., $\gamma\gamma \to \tilde{\mu}\bar{\tilde{\mu}}$). This makes easier the analysis of events with missing $p_\perp$.

5) In contrast with hadrons, a photon is pointlike, its quark content is well known. The entire photon energy is used to see the small distance phenomena of interest.

6) In some cases $e\gamma$ collisions are preferable (for example, reactions $e\gamma \to e^*$, $e\gamma \to W\nu_e^*$, $e\gamma \to \tilde{e}\tilde{\gamma}$.)

On the contrary, gauge invariance strongly constrains interactions of matter with photons. Therefore, the effects of some new interactions are suppressed here. On the other hand, it means that the originof observed effects would be separated easily.

Acknowledgement

This work is supported by grants of INTAS – 93 – 1180 and of Russian Fund of Fundamental Investigations RFFI.

References

[1] I.F. Ginzburg, G.L. Kotkin, V.G. Serbo, V.I. Telnov, Preprint 81 – 50 Inst. Nucl. Phys. Novosibirsk, 25.02.1981; Sov. ZhETF Pis'ma. 34 (1981) 514; Nucl. Instr. and Methods in Research (NIMR) 205 (1983) 47; I.F. Ginzburg, G.L. Kotkin, S.L. Panfil, V.G. Serbo, V.I. Telnov, NIMR 219 (1983) 5; V.I. Telnov, NIMR **A294**(1990) 72, see also [2,3].

[2] Proc. LBL Workshop, March 1994, NIMR **355** (1995) 1-194.

[3] Proc. Workshop on Physics and Experiments with Linear e^+e^- Colliders. Hawaii (1993) World Sc. Singapore.
[4] S.I. Polityko, Sov. Yad. Fiz. **43** (1986) 146; **56** (1993) 144.
[5] I.F. Ginzburg, G.L. Kotkin, S.I. Polityko, Sov. Yad. Fiz. **37** (1983) 368; **40** (1984) 1495; Phys. At. Nucl.**56** (1993) 1487.
[6] V. Shiltsev. Private communication.
[7] Proc. 9th International Workshop on Photon-Photon Collisions, San Diego (1992) World Sc. Singapore.
[8] P. Chen, T. Barklow, M. Peskin, Phys. Rev. **D49** (1994) 3209; R. Engel et al., see below.
[9] Budnev V.M., I.F.Ginzburg, G.V.Meledin & V.G.Serbo, Phys.Rep. **15C** (1975) 181.
[10] I.F. Ginzburg, D.Yu. Ivanov. Submitted to Phys. Rev. **D**
[11] I.F. Ginzburg, et al., Nucl.Phys. **B284** (1987) 685; **B296** (1988) 569.
[12] I.F. Ginzburg and D.Yu. Ivanov, Nucl. Phys. B (Proc. Suppl.) **25B** (1992) 224; Nucl.Phys. **B388** (1992) 376.
[13] A.D.Mueller Nucl. Phys. **B415** (1994) 373.
[14] D.Yu. Ivanov. Phys. Rev. **D**, in print.
[15] V.E. Balakin, I.F. Ginzburg, in ref. [3].
[16] D.L. Borden, D.A. Bauer, D.O. Caldwell, Phys. Rev. **D48** (1993) 4018.
[17] V. Khoze, in Proc. Sheffield Workshop on Photon–Photon Collisions, April 1995.
[18] G. Jikia, A. Tkabaladze, NIMR **A355** (1995) 81.
[19] D.A. Morris, T.N. Truong, D. Zappala, Phys. Lett. **B323** (1994) 421.
[20] E.E. Boos, et al., Zeit. Phys. **C56** (1992) 487.
[21] I.F. Ginzburg, Preprint TP 28 (182) Inst. of Mathem. Novosibirsk (1990).
[22] I.F. Ginzburg, Sov.Yad.Fiz. (Phys. At. Nucl.) **58** (1995) 326.
[23] G. Belanger, F. Boudjema, I.F. Ginzburg, in preparation.
[24] I.F. Ginzburg, G.L. Kotkin, S.L. Panfil, V.G. Serbo, Nucl. Phys. **B228** (1983) 285, E.: **B243** (1984) 550.
[25] I.F. Ginzburg, et al., Sov.Yad.Fiz. **56** (1993) 39.
[26] I.F. Ginzburg, V.A. Ilyin, A.E. Pukhov, V.G. Serbo, In preparation.
[27] G. Jikia, NIMR **A355** (1995) 84.
[28] A. Aeppli, F. Cuypers, G.J. van Oldenborgh, Phys.Lett. **B314** (1993) 413
[29] M. Veltman, Physica **29** (1963) 186; R.G. Stuart, Phys.Lett. **B262** (1991) 113; preprint UM-TH-95-13; A. Sirlin, Phys. Rev. Lett. **67** (1991) 2127; H. Veltman, DESY 92-076 (1992).
[30] "Tests of alternative models at a 500 GeV NLC", eds. F.Boudjema and F.M.Renard, ENSLAPP-A-365/92 (1992).
[31] S.Y.Choi, F.Shrempp, Phys. Lett. **B272** 149; E.Yehudai, SLAC-Report-383 (1991).
[32] F.Boudjema et al., Phys. Rev. **D43** (1991) 3683.
[33] K.Hikasa in Proc. 2-nd Workshop on JLC, KEK 91–10 (1991).
[34] G. Jikia, Phys.Lett. **B298** (1993) 224; Nucl.Phys. **B405** (1993) 24; G. Jikia, A. Tkabaladze, Phys. Lett. **B323** (1994) 453.
[35] I.F. Ginzburg. NIMR **A355** (1995) 63.
[36] I.F. Ginzburg, in ref. [7].

3 γ spectra and backgrounds in Tesla

D. J. Schulte

DESY, Hamburg, Germany

Photon-photon physics can be studied in a linear electron-positron collider by the use of the virtual photons accompanying the beam particles as is done in storage rings. In the linear collider case the beam will be lost after the interaction anyway, so one can think of producing real photons from the beam particles and thus achieve a harder photon-photon spectrum. In addition, some of the major background sources in the electron-positron collider are due to two photon processes. These effects are increased by the production of real photons during the crossing of the bunches. While the above processes have been studied in some detail, for TESLA the investigation of the possibility of achieving high centre of mass energy photon-photon collisions has just started. In the following some preliminary estimates will be presented about the luminosity and backgrounds. For a detailed review of many relevant processes I refer to [1].

3.1 Beamstrahlung

At the interaction point of an electron-positron linear collider two sources of photons exist. The electrons and positrons are accompanied by virtual photons. In the leading logarithmic approximation, this bremsstrahlung spectrum (of quasi real photons) is given by

$$n_v(x,Q^2) = \frac{\alpha}{2\pi}\frac{1+(1-x)^2}{x}\ln\frac{Q^2(1-x)}{x^2m^2}$$

with the fine structure constant α, the electron mass m and the Q^2 scale defined by the process. The photon has a fraction x of the electrons energy.

Due to their high charge and small dimensions the bunches will produce strong electromagnetic fields. A particle traveling through the oncoming bunch of oppositely charged particles will therefore be accelerated towards the beam axis. If the fields are strong enough, the transverse bunch size will thus decrease which leads to an effective luminosity L that is larger than the geometric L_0 by the luminosity enhancement factor H_D.

$$L = H_D L_0 = H_D \frac{N^2}{4\pi\sigma_x^*\sigma_y^*} N_b f_r. \tag{1}$$

Here $\sigma^*_{x,y}$ are the transverse bunch dimension, N is the number of particles per bunch, N_b the number of bunches per train and f_r the repetition frequency with which trains are accelerated.

The bending of the trajectories will also cause the beam particles to emit photons, the beamstrahlung. This is comparable to the synchrotron radiation well known in circular

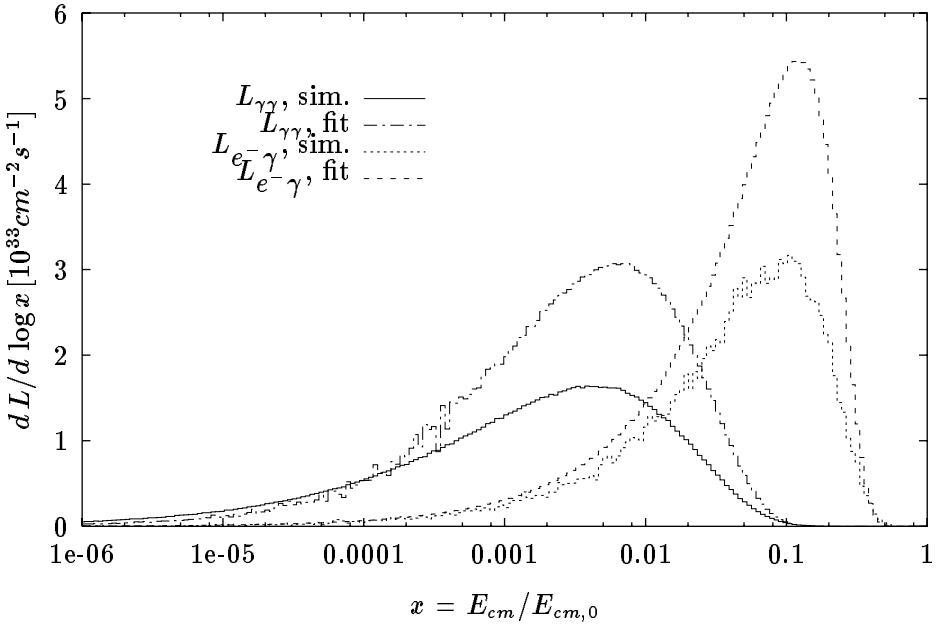

Figure 1: Comparison of half the beamstrahlung spectrum and the $L_{e\gamma}$ spectrum from the simulation and the fit.

accelerators. The average photon energy of the beamstrahlung will be of the order of a few GeV depending on the design. The beamstrahlung will cause a tail in the e^+e^--luminosity spectrum towards low energies that can be compared to the effect of initial state radiation. To suppress beamstrahlung flat beams are used. The average relative loss of energy δ is roughly proportional to $\Upsilon^2\sigma_z$ with $\Upsilon = 5Nr_e^2\gamma/(6\alpha(\sigma_x^* + \sigma_y^*)\sigma_z)$, the beamstrahlung parameter; r_e is the classical electron radius. The minimal bunch height and the bunch length σ_z are related via $\sigma_y^* \approx \sqrt{\sigma_z\epsilon_y}$, with the vertical emittance ϵ_y. This leads to

$$L \propto H_D\sqrt{\frac{\delta}{\epsilon_y}}\eta P_{AC} \tag{2}$$

where P_{AC} is the total power consumption of the accelerator and η the efficiency of turning this power into beam power. The pinch enhancement factor varies only slowly with the parameters so it can be taken as constant. The beamstrahlung will thus limit the achievable luminosity. It will in addition increase the background due to photon-photon interactions.

Since analytic calculation of the pinch effect is very difficult if not impossible, one has to simulate it. A program that also simulates the background processes is GUINEA-PIG [2]. It was used for all following calculations.

The current TESLA parameters are $\sigma_x^* = 850\,nm$, $\sigma_y^* = 19\,nm$, $\sigma_z = 700\,\mu m$, $\gamma\epsilon_x = 14\cdot 10^{-6}\,m$, $\gamma\epsilon_y = 0.25\cdot 10^{-6}\,m$, $N = 3.63\cdot 10^{10}$, $N_b = 1135$ and $f_r = 5\,Hz$. This leads to $\delta \approx 2.5\%$, $H_D \approx 1.6$ and $L \approx 6\cdot 10^{33}\,cm^{-2}s^{-1}$.

The beamstrahlung contributes mainly to the medium energy photon spectrum around

a few GeV. Since for small energies it shows a $x^{(-2/3)}$ behaviour, it is small compared to the virtual photon spectrum while at high energies it is exponentially suppressed. In [3] an approximate formula for the beamstrahlung spectrum based on simulation results was derived. Figure 1 shows the agreement between this formula and the simulation in the case of TESLA.

3.2 Background

3.2.1 Pair Production

Two sources of pair production exist. In the coherent process a photon turns into an electron-positron pair in a strong external field. This source is exponentially suppressed for small beamstrahlung parameters. Its contribution to the total number and energy of the pairs can be neglected in the case of TESLA.

In the incoherent process the pair is produced in a two photon collision: $\gamma\gamma \to e^+e^-$. To this process the real photons from beamstrahlung contribute as well as the virtual photons from the beam particles. Averaging over the polarizations in the initial state and summing over the polarizations in the final state the cross section is given by

$$\frac{d\sigma}{dt} = \frac{2\pi r_e^2 m^2}{s^2}\left[\left(\frac{t-m^2}{u-m^2}+\frac{u-m^2}{t-m^2}\right) - 4\left(\frac{m^2}{t-m^2}+\frac{m^2}{u-m^2}\right) - 4\left(\frac{m^2}{t-m^2}+\frac{m^2}{u-m^2}\right)^2\right], \quad (3)$$

where s, t and u are the Mandelstam variables.

The produced particles are deflected by the fields of the beams. After the interaction most of them have either a small angle with respect to the beam axis or a small transverse momentum. With the help of an external solenoidal field they can thus be trapped in conical masks with small opening angles. A small number will have a large transverse momentum and a relatively large angle from the production. These can hit the detectors, especially the vertex detector.

3.2.2 Hadrons and Minijets

The two photon collisions will lead to the production of hadrons. The dependence of the hadronic cross section on the centre of mass energy of the photons is not known. A reasonable assumption may be to scale the two hadron total cross sections down. The two photon cross section can then be expressed as $\sigma_{\gamma\gamma} \approx \sigma_{\gamma p} \cdot \sigma_{\gamma p}/\sigma_{pp}$. This assumption leads to [4]

$$\sigma_{\gamma\gamma} \;=\; 200\,nb\left[1 + 6.3\cdot 10^{-3}\ln^{2.1}\frac{s}{GeV^2} + 1.96\left(\frac{s}{GeV^2}\right)^{-0.37}\right].$$

The dynamics of photon-photon collisions both in the soft and hard regime (e.g. jet production) is discussed in more details below [5]. Here, our results are based on cal-

culations in the leading logarithmic approximation using the Drees and Grassie (DG) parametrization of the photon structure function.

3.2.3 Results

The total number of background electrons and positrons produced per bunch crossing is $N_{e^+e^-} \approx 1.0 \cdot 10^5$ with a total energy of $E_{e^+e^-} \approx 1.5 \cdot 10^5\, GeV$. The number of hadronic events with a centre of mass energy of more than $5\, GeV$ expected is $N_H = 0.16$. The number of minijets with a transverse momentum $p_\perp > 3.2\, GeV/c$ is $N_{MJ} = 0.4 \cdot 10^{-2}$ using the DG-parametrization. During the time of about $700\, ns$ between two bunch crossings within a train, most of the detectors could be read out.

3.3 Photon-Photon Collider: Basic Idea

The virtual photon spectra provide high centre of mass energy photon-photon collisions with only a limited luminosity. If one is for example interested only in two photon events with 60% of the nominal centre of mass energy one will have $L_{\gamma\gamma} \approx 5 \cdot 10^{-4} L$. The beamstrahlung does not improve this. In the case of TESLA the additional photon-photon luminosity is smaller by additional six order of magnitude. A method to achieve harder photon spectra is the use of backward Compton scattering. In this method two electron beams are focussed as for electron-positron collision. At some distance d from the interaction point in the conversion region one lets the electrons collide with a very dense laser beam. The backscattered hard photons will move in direction of the incident electron and thus provide the required photon-photon luminosity in the interaction point.

To prevent the electron beams, after conversion, from contributing to the luminosity in the interaction point, one could use a small dipole magnet that gives them an angular kick. It could also be possible to use a plasma lens after the conversion that will over focus the beam. It will then be very dilute at the interaction point. Another method is simply to let the beams collide. Since both bunches consist of electrons they will deflect each other thus naturally decreasing the luminosity.

3.4 Compton Scattering

The differential cross section for Compton scattering is given by

$$\frac{d\sigma}{dx} = \frac{2\pi r_e^2}{x}\left[\frac{1}{1-y} + 1 - y - 4r(1-r) + 2\lambda P r x (1-2r)(2-y)\right] \qquad (4)$$

where $x(mc^2)^2$, related to the square of the centre of mass energy ($x(mc^2)^2 = s - m^2$), is $x(mc^2)^2 = 4\hbar\omega_L E_0 \cos^2(\theta_0/2)$ with $\hbar\omega_L$ the energy of the laser photon and E_0 that of the electron. The crossing angle between electron and laser beam is θ_0, $yE_0 = \hbar\omega$ the energy of the backscattered photon and $r = y/(x(1-y))$ is introduced for convenience.

The helicity of the electron is λ and the polarization of the photon P. For $\lambda P = 0$ the spectrum is slightly peaked at the maximal photon energy. For $\lambda P = -1/2$ the peak will become more enhanced while the high energy part of the spectrum will be suppressed for $\lambda P = 1/2$. Polarization of the electron as well as the laser photon beam will thus be advantageous and result in a luminosity spectrum with a higher peak at the maximal centre of mass energy. The polarization of the hard part of the backscattered photon spectrum will also improve.

The maximal energy of the backscattered photons $\hat{E}_\gamma$ depends on the electron E_0 and laser photon energy as $\hat{E}_\gamma = y_m E_0$ with $y_m = x/(x+1)$. To achieve the largest centre of mass energy the photon energy should thus be maximal. If on the other hand $\hbar\omega\hbar\omega_L > 4(mc^2)^2$ the hard Compton photons and the laser photons can produce pairs via the incoherent process. The cross section is comparable to the Compton cross section. To suppress the pair production one can require $y_m x < 4$. This leads to $x < 2\left(1+\sqrt{2}\right) \approx 4.8$ and in turn to $y_m \approx 0.83$. For $E_0 = 250\,GeV$ the required laser photon energy would thus be $\hbar\omega_L \approx 1.25\,eV$.

3.5 Conversion

The required soft photons can be produced with a laser. The details of the conversion and the choice of parameters for the laser beam will depend on the technology used.

3.5.1 Thickness of the Laser Target

For an unlimited laser power one can assume the laser beam to be longitudinally and transversely uniform. The conversion can be described with the help of k_L, the laser target thickness in number of interaction lengths. The probability that an electron will at least scatter once, the conversion efficiency, is given by $k = 1 - \exp(-k_L)$. The scattered electrons can scatter again producing softer Compton photons. Since the cross section is increasing for smaller centre of mass energies the produced soft tail of the photon spectrum will increase faster than the high energy peak. The thickness chosen for the laser target has thus to be a compromise between required efficiency and the sharpness of the spectrum

In a more precise model the collision between the laser beam and the electron beam can be described as any beam-beam collision without pinch effect. The laser beam emittance in this case is $\epsilon_\gamma = \lambda/(4\pi)$. A reasonable approach is to choose the laser bunch length and its beta function β_γ to be of the same order as the electron bunch length. The resulting spot size will in the present case be much larger than the transverse dimension of the electron beam, so that in the case of head on collision the target is indeed transverly almost uniform. Longitudinally, there is some difference but the effect on photon-photon luminosity spectrum is not very strong.

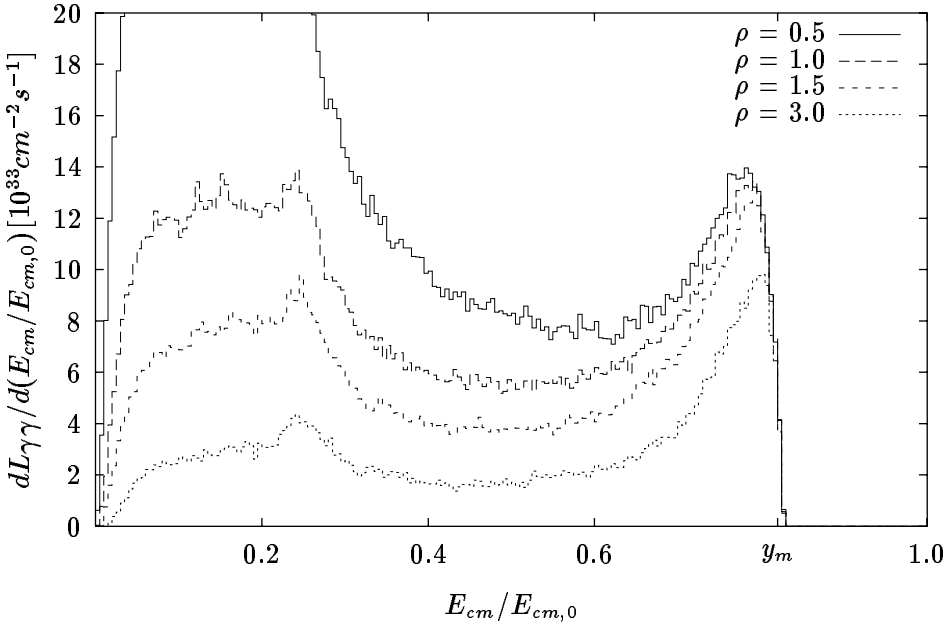

Figure 2: The photon-photon centre of mass spectrum for different distances ρ between the conversion region and the interaction point.

3.5.2 Monochromatization of the Spectrum

The backscattered photons will have small angles θ_γ with respect to the direction of motion of the initial electron. These angles are of the order of mc^2/E_0 and depend on the energy of the backscattered photon:

$$\theta_\gamma(y) = \frac{mc^2}{E_0}\sqrt{\frac{x-(x+1)y}{y}}.$$

Without this angle the photon-photon luminosity would be simply $L_{\gamma\gamma} \approx L_0 n_\gamma^2$, where n_γ is the average number of backscattered photons per incoming beam particle. The luminosity would differ slightly from the geometric because the transverse dimensions of the bunch change over its length.

The scattering angle leads to a dependence of the luminosity on the distance between the interaction point and the conversion region. Since the low energy photons have larger angles than the hard ones the luminosity for the former will decrease faster with the distance than for the latter. A convenient dimensionless parameter to describe the distance is $\rho = dmc^2/(E_0\sigma_y)$. Figure 2 shows the dependence of the absolute luminosity spectrum for a target thickness of one conversion length and several distances. The parameters of the collider in this case are the ones for TESLA discussed below. A perfect beam polarization and no contribution of the electron bunches to the luminosity was assumed.

3.6 Luminosity and Choice of Parameters

To find a reasonable parameter set for the photon-photon version of TESLA it is sensible to start from the e^+e^--parameters. The $\gamma\gamma$ luminosity will be approximately proportional to the geometric luminosity which should therefore be maximized. In equation 1 the factor NN_bf_r is proportional to the beam energy which in turn is proportional to the total power consumption of the linac. Assuming that this value is the same as for the e^+e^--option and thus fixed, the geometrical luminosity is proportional to the charge per bunch and inversely proportional to the transverse dimensions. Since these dimensions are given by $\sigma = \sqrt{\epsilon\beta}$, with ϵ the emittance and β the beta function at the interaction point, one can in principle lower either the emittance or the beta-function. Since an e^+e^--machine profits from a small vertical emittance the same way a photon-photon collider does one should assume this value the same for both options. A reduction of the vertical beta function will lead to a slightly increased luminosity but one will be limited by the hourglass effect and the Oide limit. The first is simply due to the fact that in order to achieve the small spot size the angular spread of the beam particles has to be large so that the bunch transverse dimensions will change significantly over its length. During the collision the bunches will therefore look like a hourglass. The Oide effect is due to the energy loss of the particles in the final magnets that will lead to focusing different from the nominal. With the help of an additional magnet which reduces the Oide effect and shorter bunches which reduce the hourglass effect it is possible to achieve a vertical bunch size of $\sigma_y \approx 10\,nm$ [7]. In the following the vertical bunch size is the same as in the electron-positron collider. For the

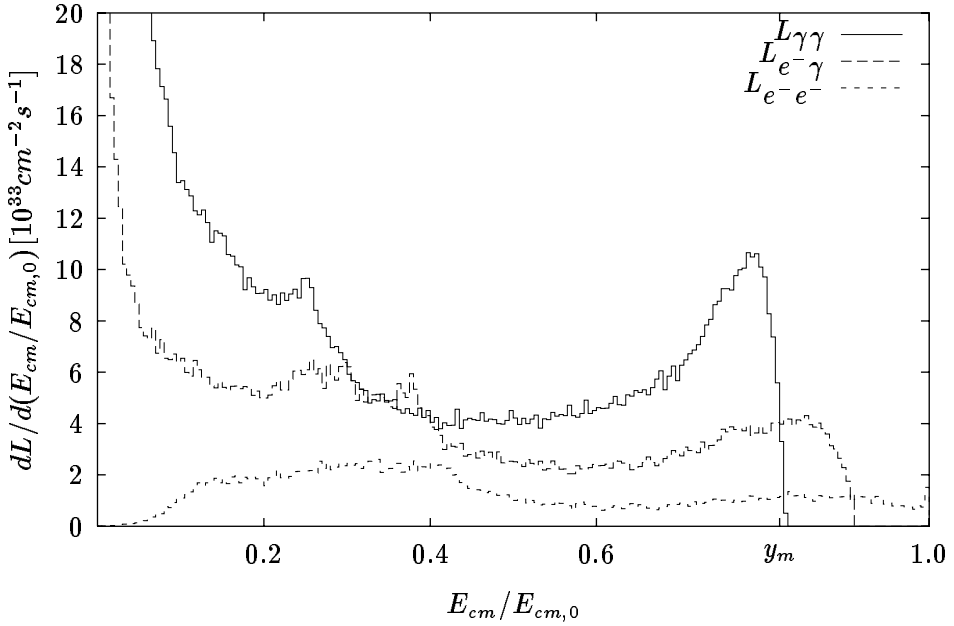

Figure 3: The photon-photon, electron-photon and electron-electron centre of mass spectrum for the TESLA parameters as described in the text.

horizontal dimension the case is completely different. The lower limit for σ_x is not given by the emittance at the e^+e^--machine but by the beamstrahlung. If one needs not care about

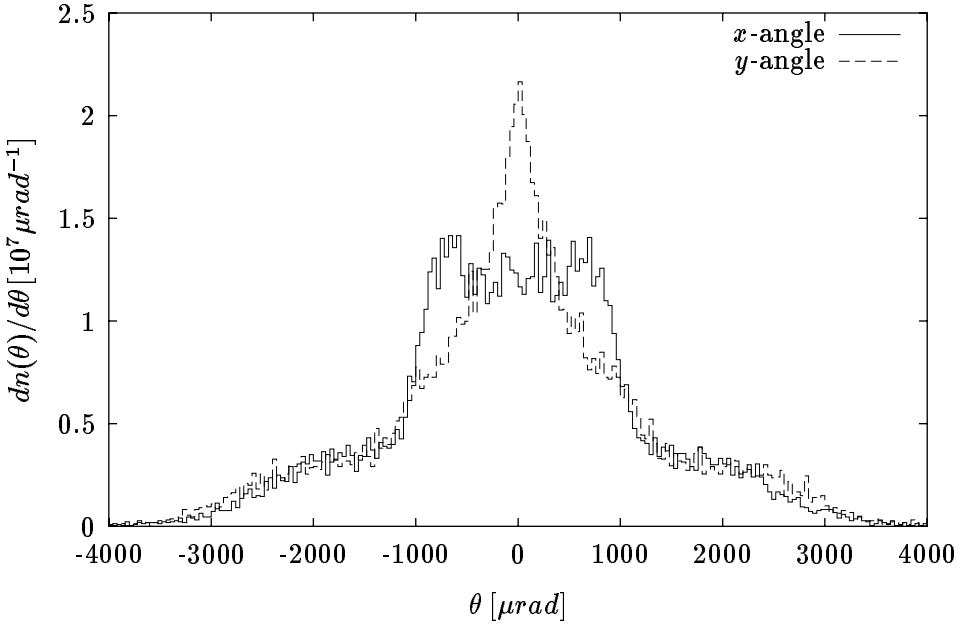

Figure 4: The angular electron distribution after the interaction point for the same case as in the previous figure.

this effect, σ_x can be reduced by a factor of two simply by reducing the beta function. In addition one can think of decreasing the horizontal emittance, which does not help for the e^+e^--machine and is thus not advocated strongly there. A reduction of the emittance by a factor two seems feasible, leading to a horizontal spot size of $\sigma_x \approx 200\,nm$ [8]. The third option is to increase the bunch charge. This has the disadvantage that the blow up of the vertical emittance $\Delta\epsilon_y$ in the linac due to single bunch wake fields will increase since $\Delta\epsilon_y \propto N^2$. While $\Delta\epsilon_y$ is small in TESLA one can nevertheless think of using this option but careful studies have to be done.

3.7 Results

The Compton scattering was simulated for the above mentioned approximations for a beam polarization of 80%. The resulting photons and electrons were transported to the interaction point and used as an input for the beam-beam simulation programme GUINEA-PIG. As a first idea the following parameters were used: $\rho = 1.5$, $k_L = 1$, $\sigma_x^* = 200\,nm$, $\sigma_y^* = 19\,nm$, $\sigma_z = 700\,\mu m$, $\gamma\epsilon_x = 7 \cdot 10^{-6}\,m$, $\gamma\epsilon_y = 0.25 \cdot 10^{-6}\,m$, $N = 3.63 \cdot 10^{10}$, $N_b = 1135$ and $f_r = 5\,Hz$. No separation of the beams was assumed. Figure 3 shows the resulting luminosity spectra for photon-photon, photon-electron and electron-electron scattering. The resulting photon-photon luminosity with a centre of mass energy of more than $300\,GeV$ is about $L_{\gamma\gamma} \approx 1.6 \cdot 10^{33}\,cm^{-2}s^{-1}$. The total photon-photon luminosity is roughly $9.1 \cdot 10^{33}\,cm^{-2}s^{-1}$, $L_{e^-\gamma} = L_{\gamma e^-} = 4.7 \cdot 10^{33}\,cm^{-2}s^{-1}$ and $L_{e^-e^-} = 1.3 \cdot 10^{33}\,cm^{-2}s^{-1}$. The first source of backgrounds will be the conversion region. Since the dependence of most of these backgrounds on the actual layout and the laser used is

significant it will not be considered here. Another very important source of background may come from the so called spent beam that is the beam behind the interaction point. The angular distribution may become rather large, see figure 4. This also depends very much on the layout of the detector. Both backgrounds mentioned will need detailed study. In the following only the backgrounds produced in the interaction point will be considered. They can be calculated using the same way as for the electron-positron machine.

The values found are $N_{e^+e^-} \approx 87 \cdot 10^3$, $E_{e^+e^-} \approx 3.2 \cdot 10^6\, GeV$, $N_H \approx 0.62$, $N_{MJ}(p_\perp > 3.2\, GeV/c) \approx 0.27$ and $N_{MJ}(p_\perp > 10.0\, GeV/c \approx 5.4 \cdot 10^{-3}$.

References

[1] V. Telnov, NIM **A 355** (1995) 3.
[2] D. Schulte, thesis, in preparation.
[3] P. Chen, Phys. Rev. **D 46** (1992) 1186.
[4] P. Chen, T. L. Barklow and M. E. Peskin, SLAC-PUB-5873.
[5] R. Engel et al., see next section.
[6] M. Drees and K. Grassie, Z. Phys. **C 28** (1985).
[7] R. Brinkmann, private communication
[8] O. Napoly, private communication.

4 Kinematical coverage for determining the photon structure function F_2^γ

D.J. Miller[1], A. Vogt[2]

[1] *University College, London, Great Britain* [2] *DESY, Hamburg, Germany*

In this section we briefly address the potential of a high–energy linear collider for measuring the photon structure function. See ref. [1] for a discussion at the previous linear collider workshop. We will restrict ourselves to an e^+e^- center-of-mass energy of $\sqrt{s} =$ 500 GeV. With respect to the electroweak part of the process, we will consider only the electromagnetic one-photon-exchange process, i.e. we assume that radiative corrections and contributions due to the exchange of weak bosons have been subtracted.

It is convenient for the following discussion to recall the basic kinematics of deep–inelastic lepton–photon scattering in e^+e^- collisions in this approximation. In Fig. 5a the so-called 'single–tag' situation is shown, where the electron or the positron is detected at some $\theta_{tag} > \theta_0$, with a veto against a second tag anywhere in the detector covering $\theta_0 < \theta < \pi - \theta_0$. The generalization to 'double–tag' events is obvious, such events will however play no role at the linear collider. θ_0 is an essential apparative parameter for the kinematical coverage and event rates for structure function measurements.

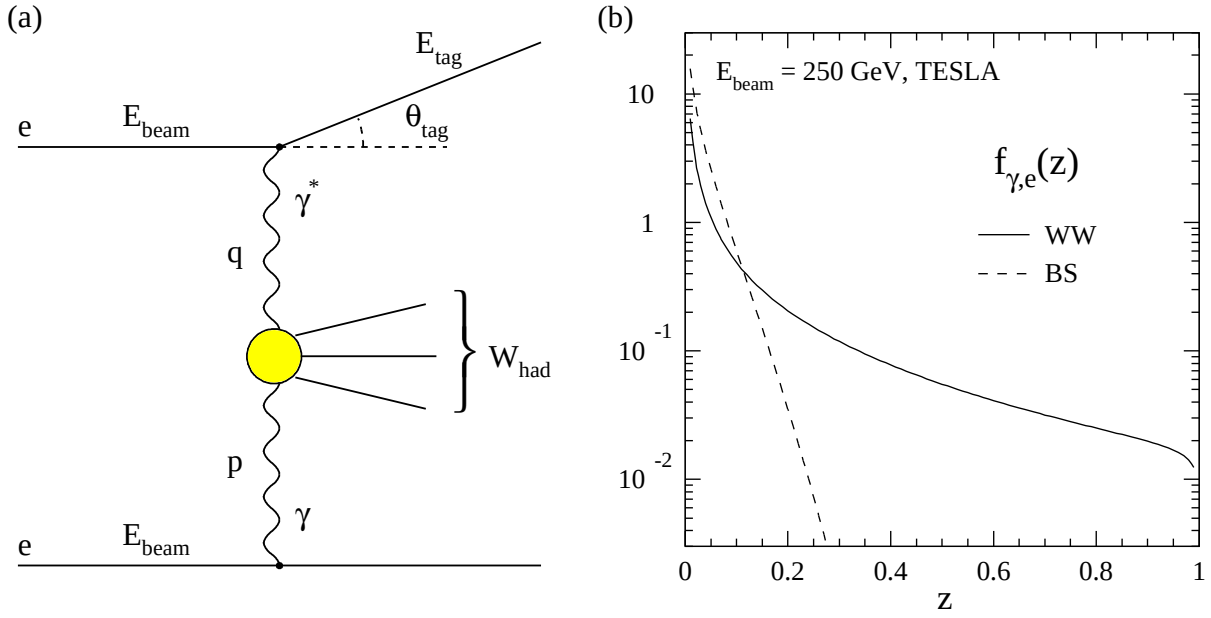

Figure 5: **(a)** The kinematics of a single–tag inclusive $\gamma\gamma$ event. **(b)** The flux functions for Weizsäcker–Williams (WW) bremsstrahlung and beamstrahlung (BS) photons at a 500 GeV linear collider. In the WW case the emitting electron is assumed to be anti-tagged with $\theta_0 = 40$ mr; the BS parameters are $\Upsilon = 0.039$ and $\sigma_z = 500\,\mu$m.

The cross section for (unpolarized) inclusive lepton–photon scattering reads to lowest

order in the electromagnetic coupling α:

$$\frac{d\sigma(e\gamma \to eX)}{dE_{tag}\, d\cos\theta_{tag}} = \frac{4\pi\alpha^2 E_{tag}}{Q^4 y}\left[\{1+(1-y)^2\}F_2^\gamma(x,Q^2) - y^2 F_L^\gamma(x,Q^2)\right] . \qquad (5)$$

Here $F_{2,L}^\gamma(x,Q^2)$ denote the structure functions of the real photon. The virtuality of the probing photon and the invariant mass of the (hadronic) final state are given by

$$Q^2 \equiv -q^2 = 2E_{beam}E_{tag}(1-\cos\theta_{tag}) , \qquad W_{had}^2 = (q+p)^2 , \qquad (6)$$

and we have introduced the usual dimensionless variables

$$x = \frac{Q^2}{Q^2+W_{had}^2} , \qquad y = 1 - \frac{E_{tag}}{E_{beam}}\cos^2\left(\frac{\theta_{tag}}{2}\right) . \qquad (7)$$

Experimentally E_{tag} is restricted by background suppression cuts, typically at least to $E_{tag} > 0.5\, E_{beam}$. Hence Q^2 is limited by eq. (6) to $Q^2 \gtrsim 0.5\, E_{beam}^2\, \theta_0^2$, which in turn restricts the reach towards small x via eq. (7). Moreover, the left hand side of eq. (5) is then entirely dominated by F_2^γ. We will confine ourselves to the prospects for measuring this quantity in what follows.

In order to yield the experimentally observable cross section, eq. (5) has to be convoluted with the flux $f_{\gamma,e}(z = E_\gamma/E_{beam})$ of the incoming photons. Firstly, we will study the case of the standard Weizsäcker–Williams (WW) spectrum [2] for the quasi-real photons emitted by the anti-tagged electron, see eq. (22) in Section 6.1.1. This leads to a high-P^2 tail up to $P_{max}^2 \simeq (1-z)\, E_{beam}^2\, \theta_0^2$ for the target photon virtuality $P^2 \equiv -p^2$, which has to be corrected for in determinations of $F_2^\gamma(x,Q^2)$. Secondly, we will consider the case of real-photon beamstrahlung (BS) [3] for the TESLA design of the linear collider. In this case we take the approximate expression and parameters for the BS spectrum as given in Section 6.1.2, eqs. (24)–(26). The two spectra are compared in Fig. 5b. Note the very soft energy distribution of the BS photons for this design.

A possible option at a linear collider which is especially well suited for photon structure function measurements is the conversion of one of the electron beams to a photon beam by backscattering of laser photons (BL) [4]. Under suitable polarization conditions a rather monochromatic photon beam, $\Delta E_\gamma \approx 0.1\, E_\gamma$, with $E_\gamma \simeq 0.8 E_{beam}$ can be obtained in this way. For our purpose a rough approximation of the actual momentum spectrum is sufficient, we have taken $f(z) = 375(z-0.63)^2$ for $0.63 \le z \le 0.83$, and $f(z) = 0$ else, for our simulations discussed below.

The fact that the momentum p of the (quasi-)real photon is unknown in the WW and BS cases leads to a key systematic problem in the measurement of the photon structure functions: W_{had} in eq. (6) and hence x in eq. (7) cannot by determined from the outgoing electron alone, in contrast to the situation in the BL $e\gamma$ mode and usual (electromagnetic) lepton–nucleon deep–inelastic scattering. Thus the measurement has to rely on the hadronic final state, of which however in general only a part W_{vis} of the invariant mass is seen in the calorimeters. The resulting problem of reconstructing W_{had} from W_{vis} is especially severe at high W_{had}, i.e. at small-x [5].

It is useful to recall what can be maximally done on F_2^γ before the linear collider becomes operational, i.e. at LEP2 [6]. Here the minimum angle of the main detector coverage is about $\theta_0 \simeq 30$ mr due to synchrotron radiation shielding masks. Therefore Q^2 is limited to the region $Q^2 \gtrsim 3.5$ GeV^2, kinematically allowing for measurements down to about $x \approx 5 \cdot 10^{-4}$. Since here the photon remnant can be expected to be measureable to a large extend in the forward calorimeters, a sufficient correlation between W_{vis} and W_{had}, allowing for an unfolding of $F_2^\gamma(x, Q^2)$ at small x, should be possible. With respect to high Q^2, the structure function measurement at LEP2 will run out of statistics at a few hundred GeV^2. The resulting maximal potential of LEP2 is illustrated in Fig. 6.

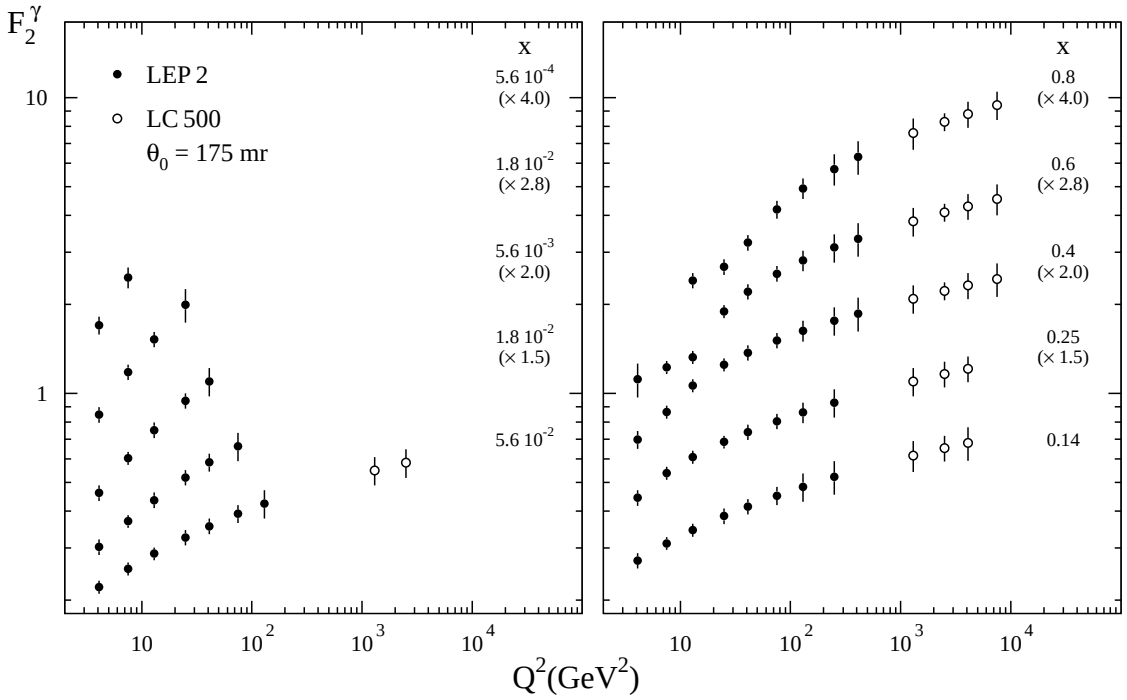

Figure 6: The kinematical coverage and maximal accuracy of the measurement of F_2^γ at LEP2 and at a 500 GeV linear collider, in the latter case assuming that electron tagging is only possible outside the shielding masks at about 10 degrees. See the text below the next figure for a discussion of the error estimates.

At the linear collider, the radiation shielding masks are expected to be located at about 10 degrees. A minimal scenario is to assume that electron tagging will be possible only outside this shielding, i.e. $\theta_0 = 175$ mr. The maximally possible F_2^γ measurements using the WW spectrum for this case are compared to the corresponding LEP2 expectation in Fig. 6. Under these circumstances, all one obtains are some 5000 events at 'high' x in the previously unaccessible range $Q^2 > 1000$ GeV^2. Hence no overlap with the LEP2 results can be achieved, which would allow for adjusting the relative normalizations of the measurements. It should be noted that, at least for the TESLA design considered here, beamstrahlung cannot very much improve the situation with respect to statistics, due to the softness of its energy spectrum shown in Fig. 5b.

Consequently for an F_2^γ determination with wide kinematical coverage and high pre-

cision, electron tagging inside the shielding is mandatory. Expected event numbers for the measurement of $F_2^\gamma(x,Q^2)$, are given in Fig. 7 in bins in x and Q^2 for $\theta_0 = 40$ mrad, resulting in $Q^2_{min} = 50$ GeV^2, for both the WW and BS cases. If this can be achieved practically, a precise measurement overlapping with LEP2 results is possible, taking over with high statistics at $Q^2 \simeq 100$ GeV^2 where the accuracy at LEP2 begins to degrade. Also in this case beamstrahlung does not appreciably modify the kinematical coverage and expected accuracies, as it increases the number of events significantly only where enough statistics is already expected.

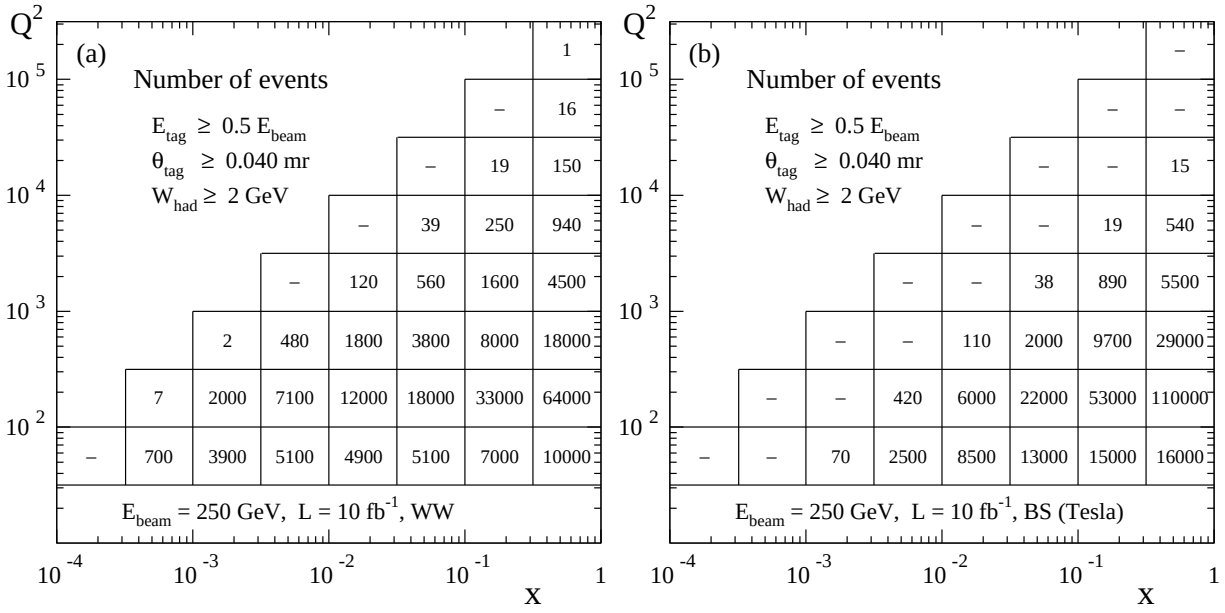

Figure 7: The expected number of events for the determination of F_2^γ at a 500 GeV linear collider in case that electron tagging well inside the shielding is possible. In **(a)** the standard anti-tag WW photon spectrum has been used $\theta < 40$ mr, and **(b)** is the same for the TESLA BS case. Q^2 is given in GeV^2.

The event numbers in Fig. 7 have been calculated using the leading order (LO) GRV parametrization of the photon's parton densities [7], together with the LO $\gamma^*\gamma \to c\bar{c}$ and $\gamma^* g \to c\bar{c}$ Bethe-Heitler charm contributions. See Section 8.2 for a detailed discussion of the latter processes. Only simple cuts have been applied: on E_{tag}, θ_{tag} and W_{had}. In order to account crudely for the additional suppression due to further experimental final state cuts – W_{vis} instead of W_{had}, number of tracks etc. – the nominal luminosity has been scaled down by a factor of two. The suppression of $F_2^\gamma(x,Q^2,P^2)$ with respect to $F_2^\gamma(x,Q^2)$ for the high-P^2 tail of the WW spectrum has also not been taken into account, and F_L has been neglected in eq. (5).

The corresponding maximal accuracy and kinematical coverage of the F_2^γ measurement is displayed in Fig. 8 for the WW case. Here we have simply assumed that the systematic error is equal to the statistical one inferred from Fig. 7a, but amounts to at least 5%. Shown is the quadratic sum of these two contributions. The errors shown in Fig. 6 have been obtained in the same way from corresponding event number estimates not given

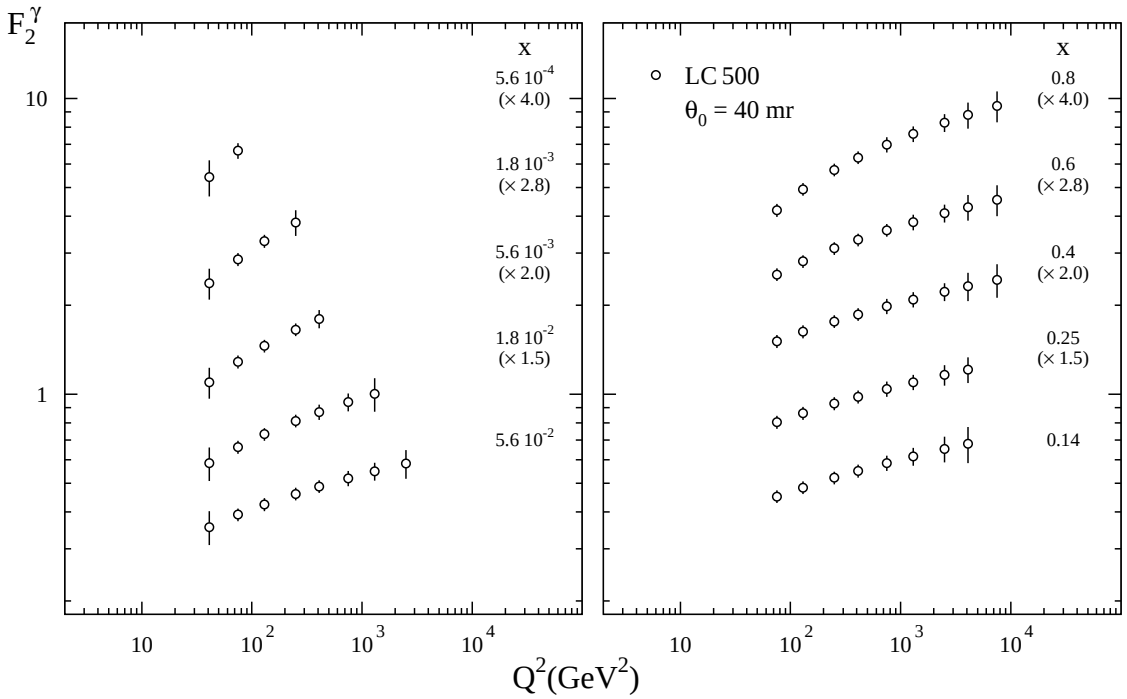

Figure 8: The kinematical coverage and maximal accuracy of the F_2^γ measurement using WW photons measurement a 500 GeV linear collider. Note that presumably no unfolding of $F_2^\gamma(x, Q^2)$ will be possible at $x < 0.1$. The values of F_2 have been multiplied be the x-dependent number indicated in brackets.

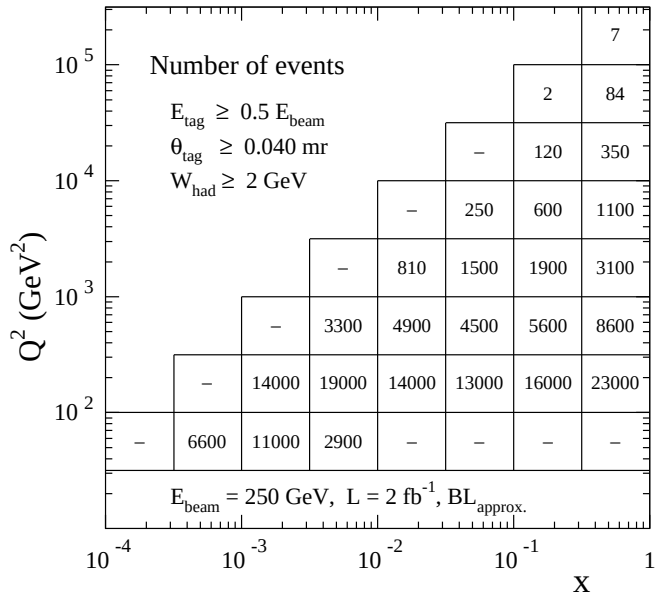

Figure 9: The expected number of events for the determination of F_2^γ in the backscattered–laser $e\gamma$ mode of a 500 GeV linear collider, assuming that 20% of the e^+e^- luminosity can be reached in this mode for a rather monochromatic photon beam.

here. See ref. [6] for the LEP2 case. With respect to the small-x region in Figs. 7 and 8 it must be noted that, unlike at LEP2, due to the higher minimum angle of the calorimetric detector coverage and the higher beam energy the bulk of the photon remnants will be lost at the linear collider. This will presumably prohibit any unfolding of F_2^γ significantly below $x \approx 0.1$.

Thus for reaching small x the $e\gamma$ mode is most probably needed. Moreover, it can be expected to allow for significantly reduced systematic errors in the regime which can be covered also in e^+e^- collisions. With respect to statistics Fig. 9 indicates that reaching about 20% of the e^+e^- luminosity in this mode is sufficient for a high-statistics measurement over almost the full range of Fig. 8. Due to the hard BL photon spectrum, there is a slight shift towards higher Q^2 and smaller x.

Let us summarize: if electron tagging inside the shielding masks at about 10 degrees is not feasible, than roughly 5000 events for F_2 in the previously unexplored high-Q^2 range can be expected. Neither overlap with LEP2 results, nor sensitivity to small-x will be obtained. To achieve this, an electron tagging device inside the shielding, down to about 40 mrad is needed. This is however still not sufficient to get measurements at small x, due to the problem of unfolding the data at very high W. In order to circumvent this problem, and also for reducing the main systematic errors at high x, the conversion to an $e\gamma$ collider by laser backscattering is the ideal mode.

Acknowledgement

This work was supported in part by the German Federal Ministry for Research and Technology under contract No. 05 6MU93P.

References

[1] D.J. Miller et al., Proceedings of the Workshop on Physics and Experiments with Linear e^+e^- Colliders, Waikaloa, Hawaii, April 1993, eds. F.A. Harris et al. (World Scientific 1993), p. 577

[2] V.M. Budnev et al., Phys. Rep. **15C** (1975) 18

[3] P. Chen, Phys. Rev. **D46** (1992) 1186;
P. Chen, T.L. Barklow and M.E. Peskin, Phys. Rev. **D49** (1994) 3209

[4] I.F. Ginzburg et al., Nucl. Inst. Meth. **A205** (1983) 47, **A219** (1984) 5;
V.I. Telnov, Nucl. Inst. Meth. **A94** (1990) 72

[5] L. Lönnblad et al., $\gamma\gamma$ generators, in the Proceedings of the Workshop on *Physics at LEP2*, CERN Yellow report, CERN 96-01, G. Altarelli, T. Sjöstrand, F. Zwirner eds.

[6] P. Aurenche et al., $\gamma\gamma$ physics, in the Proceedings of the Workshop on *Physics at LEP2*, CERN Yellow report, CERN 96-01, G. Altarelli, T. Sjöstrand, F. Zwirner eds.

[7] M. Glück, E. Reya and A. Vogt, Phys. Rev. **D46** (1992) 1973

5 The $k_\perp$ dependent gluon density of the photon

J. Blümlein

DESY, Zeuthen, Germany

In the small x range new dynamical effects are expected to determine the behaviour of structure functions. The evolution of parton densities is effected by terms due to non strong $k_\perp$ ordering. New terms besides those due to mass factorization are expected to contribute. A description of these contributions requires to generalize the factorization of the hadronic matrix elements into coefficient functions and parton densities in which the $k_\perp$ dependence is not integrated out [1]. This factorization covers the case of collinear factorization in the limit that the k^2 dependence of the coefficient function is neglected. The $k_\perp$ dependent gluon density accounts for the resummation of small x effects. Here we will consider contributions due to the Lipatov equation only. Since this equation behaves infrared finite no other singularities will emerge than those appearing in the case of mass factorization. The collinear singularities are delt with in the same way as in the case of $k_\perp$ factorization.

The $k_\perp$ dependent distribution $\Phi(x,k^2,\mu)$ can finally be represented as the convolution of the gluon density in the collinear limit $g(x,\mu)$ and a function $\mathcal{G}(x,k^2,\mu)$ for which an analytic expression will be derived.

5.1 $k_\perp$ Factorization and the $k_\perp$ dependent gluon distribution

The factorization relation for an observable $O_i(x,\mu)$ reads

$$O_i(x,\mu) = \int dk^2 \hat{\sigma}_{O_i}(x,k^2,\mu) \otimes \Phi(x,k^2,\mu) \tag{8}$$

where $\hat{\sigma}_{O_i}(x,k^2,\mu)$ and $\Phi(x,k^2,\mu)$ denote the k^2 dependent coefficient function and parton density[6], respectively. Eq. (8) can be rewritten as [2, 3]

$$O_i(x,\mu) = \hat{\sigma}^0_{O_i}(x,\mu) \otimes G(x,\mu) + \int_0^\infty dk^2 \left[\hat{\sigma}_{O_i}(x,k^2,\mu) - \hat{\sigma}^0_{O_i}(x,\mu)\right] \Phi(x,k^2,\mu) \tag{9}$$

with $\hat{\sigma}^0_{O_i}(x,\mu) = \lim_{k^2\to 0} \hat{\sigma}_{O_i}(x,k^2,\mu)$. The first term in (9) describes the conventional contribution due to collinear factorization. The second term contains the new contributions. Note that $\Phi(x,k^2,\mu)$ starts with terms $\propto \alpha_s$. It has therefore *not* the interpretation of a probability density and may even become negative.

As shown in [2] the $k_\perp$ dependent gluon distribution associated to eq. (9) reads in moment space

$$\tilde{\Phi}(j,k^2,\mu) = \gamma_c(j,\overline{\alpha}_s)\frac{1}{k^2}\left(\frac{k^2}{\mu^2}\right)^{\gamma_c(j,\overline{\alpha}_s)} \tilde{g}(j,\mu) \tag{10}$$

[6] We will consider the gluon density in the present paper only.

where μ denotes a factorization scale, $\overline{\alpha}_s = N_c\alpha_s(\mu)/\pi$, and $g(x,\mu)$ is the gluon density. Eq. (10) accounts for the small x behaviour due to the Lipatov equation. Here $\gamma_c(j,\,\overline{\alpha}_s)$ is the eigenvalue of the *homogeneous* equation obeying

$$\rho \equiv \frac{j-1}{\overline{\alpha}_s} = \chi(\gamma_c(j,\,\overline{\alpha}_s)), \quad \chi(\gamma) = 2\psi(1) - \psi(\gamma) - \psi(1-\gamma). \tag{11}$$

In x space the $k_\perp$ dependent distribution is given by the convolution

$$\Phi(x,k^2,\mu) = \mathcal{G}(x,k^2,\mu) \otimes g(x,\mu), \tag{12}$$

correspondingly, with

$$\int_0^{\mu^2} dk^2\,\Phi(x,k^2,\mu) = g(x,\mu). \tag{13}$$

The function $\mathcal{G}(x,k^2,\mu)$ is universal and can be calculated numerically by a contour integral in the complex plane over the first factor in eq. (10). Since the solution of eq. (11) is multivalued the Mellin inversion to x space requires to select the branch in which for asymptotic values of $j \in \mathcal{C}$ γ_c approaches the perturbative result $\gamma_c(j,\,\overline{\alpha}_s) \sim \overline{\alpha}_s/(j-1)$ for small values of $\overline{\alpha}_s$.

We solved eq. (11) under this condition numerically using an adaptive Newton algorithm. The solution is characterized by three branch points, see [4] for a detailed discussion and numerical results for the solution of eq. (11) for complex arguments.

5.2 An analytical solution for $\mathcal{G}(x,k^2,\mu)$

The integration contour for the Mellin transformation of $\tilde{\Phi}(j,k^2,\mu)$ to $\Phi(x,k^2,\mu)$ for $j \in \mathcal{C}$ has to be situated outside the range of the singularities of γ_c. One may expand $\gamma_c(j,\,\overline{\alpha}_s)$ into a Laurent series over ρ

$$\gamma_c(j,\,\overline{\alpha}_s) = \sum_{l=1}^{\infty} g_l \rho^{-l} \tag{14}$$

in this range.

The coefficients g_l are given in [5] up to $l = 20$ in analytical form extending an earlier result [6].

Using (14) a corresponding expansion may be performed for

$$k^2\tilde{\mathcal{G}}(j,k^2,\mu) = \gamma_c(j,\,\overline{\alpha}_s)\exp[\gamma_c(j,\,\overline{\alpha}_s)L] \tag{15}$$

with $L = \ln(k^2/\mu^2)$. For the single terms of the Laurent series in ρ the Mellin transform can be carried out analytically.

Here it is important to expand the exponential in eq. (15) in such a way that the lowest order term in $\overline{\alpha}_s$ of γ_c is *kept* in exponential form. One obtains

$$k^2\mathcal{G}(x,k^2,\mu) \;=\; \frac{\overline{\alpha}_s}{x} I_0\left(2\sqrt{\overline{\alpha}_s \log(1/x) L}\right) + \frac{\overline{\alpha}_s}{x}\sum_{\nu=4}^{\infty} d_\nu(L)\left(\frac{\overline{\alpha}_s \log(1/x)}{L}\right)^{(\nu-1)/2}$$

$$\times \quad I_{\nu-1}\left(2\sqrt{\overline{\alpha}_s \log(1/x)L}\right), L > 0. \tag{16}$$

The coefficients $d_\nu(L)$ are given in ref. [5]. Up to $\nu = 20$ they contain at most terms $\propto L^4$. The first term in eq. (16) denotes the Green's function in DLA.

For $L \to 0$ (16) takes the form

$$k^2\mathcal{G}(x,k^2,\mu) = \frac{\overline{\alpha}_s}{x}\sum_{l=1}^{\infty}\frac{g_l}{(l-1)!}\left[\overline{\alpha}_s\left(\frac{1}{x}\right)\right]^{l-1}, \tag{17}$$

and for $L < 0$ (i.e. $k^2 < \mu^2$) one has

$$\begin{aligned} k^2\mathcal{G}(x,k^2,\mu) &= \frac{\overline{\alpha}_s}{x}J_0\left(2\sqrt{\overline{\alpha}_s \log(1/x)|L|}\right) + \frac{\overline{\alpha}_s}{x}\sum_{\nu=4}^{\infty} d_\nu(L)\left(\frac{\overline{\alpha}_s\log(1/x)}{|L|}\right)^{(\nu-1)/2} \\ &\times \quad J_{\nu-1}\left(2\sqrt{\overline{\alpha}_s \log(1/x)|L|}\right). \end{aligned} \tag{18}$$

Thus for $k^2 \to 0$ damped, oscillating modes are obtained which vanish faster than $1/|L|^{-1/4}$.

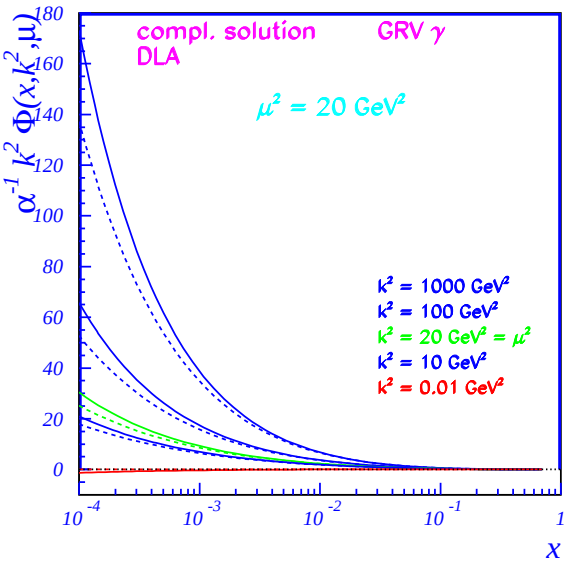

Figure 10: *The $k_\perp$ dependent gluon distribution of the photon scaled by $1/\alpha_{QED}$ as a function of k^2 and x. Full lines: complete solution; dashed lines: solution in DLA. For the input distribution $g(x,\mu)$ the parametrization [7] (LO) was used.*

The $k_\perp$ dependent gluon distribution of the photon $\Phi(x,k^2,\mu)/\alpha_{QED}$ (scaled by k^2) is shown in Fig. 10 as a function of x and k^2 for $\mu^2 = 20$ GeV^2 referring to the parametrization of ref. [7] to describe $g(x,\mu)$. The complete solution eq. (12) is larger than the DLA result for $k^2 \gtrsim \mu^2$ at $x \lesssim 10^{-3}$ by 10 to 15% while for $k^2 \to 0$ smaller values are obtained.

At larger values of x the complete solution approaches the DLA result. For $k^2 \to 0$ $\Phi(x, k^2, \mu)$ vanishes. Since the DLA result is proportional to $J_0(2\sqrt{\overline{\alpha}_s \log(1/x) \log|k^2/\mu^2|})$ for $k^2 \to 0$ a damped oscillatory behaviour is obtained in this approximation. The complete solution, on the other hand, behaves monotonous in the whole kinematical range.

Since the shape and size of the complete solution and the DLA solution are rather similar very precise measurements are required to establish the non–DLA contributions at small x although the correction is of importance numerically.

References

[1] M. Ciafaloni, Nucl. Phys. **B296** (1987) 249; S. Catani, M. Ciafaloni, and F. Hautmann, Nucl. Phys. **B366** (1991) 135.

[2] J. Collins and R. Ellis, Nucl. Phys. **B360** (1991) 3.

[3] J. Blümlein, J. Phys. **G19** (1993) 1623.

[4] J. Blümlein, in: Proc. of the XXX Rencontre de Moriond, Les Arcs, March 1995, ed. J. Tran Thanh Van (Ed. Frontières, Paris, 1996).

[5] J. Blümlein, in preparation.

[6] S. Catani, F. Fiorani, and G. Marchesini, Nucl. Phys. **B336** (1990) 18.

[7] M. Glück, E. Reya, and A. Vogt, Phys. Rev. **D46** (1992) 1973.

6 Soft, semihard and hard photon-photon physics

R. Engel[1], P. Aurenche[2], V. Del Duca[3], M. Fontannaz[4], J.Ph. Guillet[2], J. Ranft[5], T. Sjöstrand[6]

[1] *ITP, Leipzig, Germany*
[2] *ENSLAPP-Annecy, France*
[3] *DESY, Hamburg, Germany*
[4] *LPTHE, Orsay, France*
[5] *GAES, Santiago de Compostella, Spain*
[6] *DTP, Lund, Sweden*

6.1 Photon sources at linear colliders

We give here the formulae used to generate the various photon spectra in our studies of photon-photon collisions.

6.1.1 Bremsstrahlung

The flux of weakly virtual photons can be approximated taking into account only transversely polarized photons. Then, the $ee \to eeX$ photoproduction cross section is given by

$$\frac{d^2\sigma_{ep}}{dy_1 dP_1^2 dy_2 dP_2^2} = f_{\gamma,e}^{brems}(y_1, P_1^2)\, f_{\gamma,e}^{brems}(y_2, P_2^2)\, \sigma_{\gamma\gamma}(s, P_1^2, P_2^2). \tag{19}$$

with

$$f_{\gamma,e}^{brems}(y, P^2) = \frac{\alpha}{2\pi P^2}\left[\frac{1+(1-y)^2}{y} - 2m_e^2 y \frac{1}{P^2}\right]. \tag{20}$$

Here, y and $P^2 = -p_\gamma^2$ denote the energy fraction taken by the photon from the electron and the photon virtuality. m_e is the electron mass. Neglecting the dependence of the $\gamma\gamma$ cross section on P^2 in Eq. (19), the well known equivalent photon approximation [1] is obtained

$$f_{\gamma,e}^{brems}(y, P^2) = \frac{\alpha}{2\pi}\left[\frac{1+(1-y)^2}{y}\ln\frac{P^2_{\max}}{P^2_{\min}} - 2m_e^2 y\left(\frac{1}{P^2_{\min}} - \frac{1}{P^2_{\max}}\right)\right]. \tag{21}$$

Taking the kinematic limit $P^2_{\min,\mathrm{kin}} = m_e^2 y^2/(1-y)$ as lowest photon virtuality allowed one gets

$$f_{\gamma,e}^{brems}(y) = \frac{\alpha}{2\pi}\left(\frac{1+(1-y)^2}{y}\ln\frac{(1-y)}{m_e^2 y^2}P^2_{\max} - \frac{2(1-y)}{y}\right). \tag{22}$$

Given the present configuration of the e^+e^- colliders, the anti-tagging angle on the electrons or positrons will be quite large: $\theta_{max} = 175$ mrad, or may-be $\theta_{max} = 40$ mrad. This leads to large photon virtualities P^2 where the equivalent photon approximation may not be reliable. This point, which has not been studied in detail below, clearly deserves further work.

6.1.2 Beamstrahlung

In case of Gaussian beams, the effective beamstrahlung spectrum has been estimated by Chen et al. [2, 3]. The dependence of this spectrum on the particle-bunch parameters can be expressed by the beamstrahlung parameter Υ:

$$\Upsilon = \frac{5 r_e^2 E N_e}{6\alpha\sigma_z(\sigma_x^* + \sigma_y^*)m_e}. \tag{23}$$

Here, E denotes the beam energy, N_e is the number of electrons or positrons in a bunch, σ_x^* and σ_y^* are the transverse bunch dimensions, and $r_e = 2.818 \cdot 10^{-12}$mm is the classical electron radius. In our calculations we approximate the beamstrahlung spectrum by [3]

$$\begin{aligned} f_{\gamma,e}^{\rm beam}(y) &= \frac{\kappa^{1/3}}{\Gamma(1/3)} y^{-2/3}(1-y))^{-1/3}\, e^{-\kappa y/(1-y)} \\ &\cdot \left\{ \frac{1-w}{\tilde{g}(y)} \left[1 - \frac{1}{\tilde{g}(y) N_\gamma} \left(1 - e^{-N_\gamma \tilde{g}(y)} \right) \right] + w \left[1 - \frac{1}{N_\gamma} \left(1 - e^{-N_\gamma} \right) \right] \right\}, \end{aligned} \tag{24}$$

with

$$\tilde{g}(y) = 1 - \frac{1}{2}(1-y)^{2/3} \left[1 - y + (1+y)\sqrt{1 + \Upsilon^{2/3}} \right] \tag{25}$$

and $\kappa = 2/(3\Upsilon)$, $w = 1/(6\sqrt{\kappa})$. The average number of photons N_γ emitted per electron is given by

$$N_\gamma = \frac{5\alpha^2 \sigma_z m_e}{2 r_e E} \frac{\Upsilon}{\sqrt{1 + \Upsilon^{2/3}}}. \tag{26}$$

Here we use $\Upsilon = 3.9\ 10^{-2}$ and $\sigma_z = 500\mu$m, slightly different from the values discussed in [4].

6.1.3 Photon emission by laser-backscattering

Depending on the polarization of the laser light, various photon spectra can be produced [5]-[7]. In the following, only the case of unpolarized electrons and unpolarized laser radiation is considered. If the laser frequency is chosen according to the optimal value $x_c = 2 + \sqrt{8}$ given in [7], the spectrum of the photon flux can be approximated by

$$f_{\gamma,e}^{laser}(y) = \frac{-0.544\ y^3 + 2.17\ y^2 - 2.63\ y + 1.09}{(1-y)^2}\ \Theta(0.828 - y). \tag{27}$$

6.2 Photon-photon cross section predictions

In the following, cross section predictions of a few models are presented. Details about the models used here can be found elsewhere (PYTHIA [8, 9], PHOJET [10, 11], eikonalized minijet model [12]). A discussion of some uncertainties in estimating the inelastic cross

section is given in the next section [12]. All the models are using unitarization schemes to avoid the violation of unitarity at high energies.

Since the total cross section cannot be calculated using only perturbative QCD, several model dependent assumptions are necessary. The models start to determine the free parameters by fits to total, elastic and diffractive cross section of proton-proton/antiproton collisions. The results of the fits depend on the choice of the parton structure functions and cutoffs for the minijet component. Assuming Regge factorization, one proton is substituted by a photon keeping the couplings and parameters belonging to the proton side the same as in proton-proton collisions. This substitution introduces new free parameters corresponding to photon specific properties. These parameters are determined by fitting the total photoproduction cross section and the cross section on quasi-elastic ρ^0 production. Once the model parameters are fixed, photon-photon cross sections can be predicted without introducing new arbitrary parameters. In Fig. 11 the inelastic photon-photon cross section according to PYTHIA, PHOJET and the eikonalized minijet model is shown together with data. Since there is little known about the low-x behaviour of the

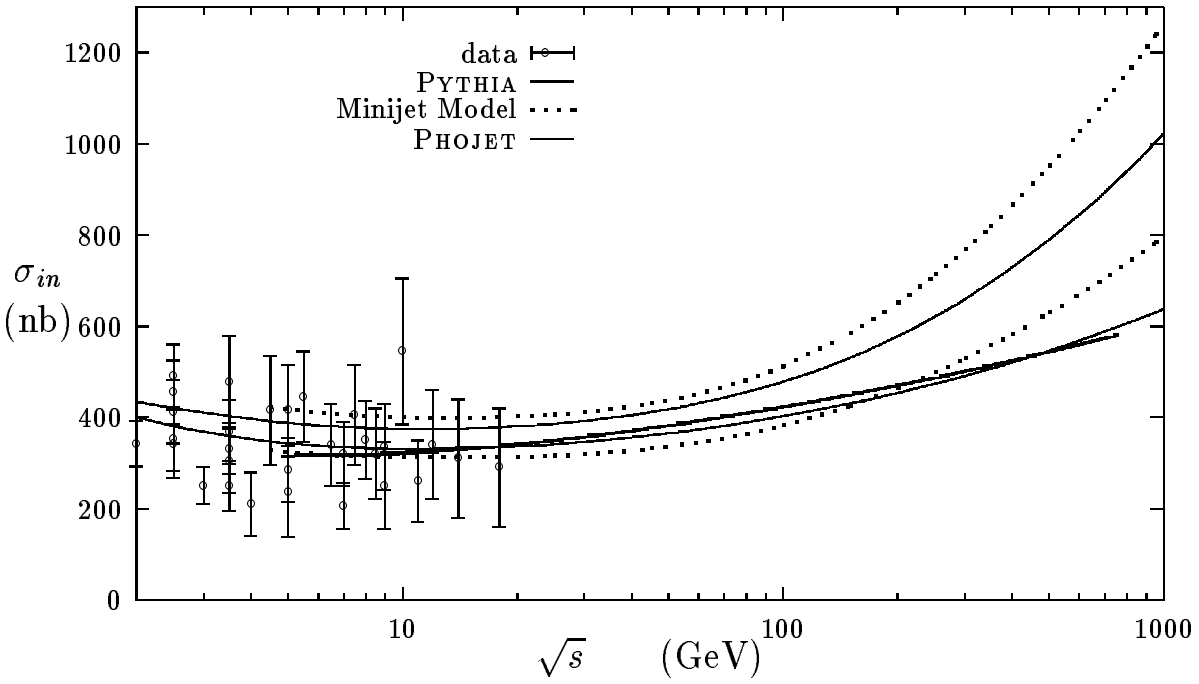

Figure 11: Inelastic photon-photon cross sections calculated with the models PYTHIA [8, 9], PHOJET [10, 11] and an eikonalized minijet model [12] are compared with data. The two curves from PHOJET were calculated using the GRV LO photon structure function [13] (upper curve) and the SaS 2M photon structure function [14] (lower curve). The two curves according to the unitarized minijet model are the highest and the lowest prediction presented in [12].

photon structure function, the predictions of the models at high energies depend strongly on the parton distributions assumed for the photon. A somewhat more optimistic picture is provided by VMD scenarios, where the small-x behaviour of parton distributions and hence the energy dependence of the $\gamma\gamma$ cross section is expected to be qualitatively similar to the observed $p\bar{p}$ ones.

6.3 Photon-photon hadron production

6.3.1 General characteristics

It is expected that photon-photon scattering at high energies behaves similar to hadron-hadron interactions. However, due to the dual nature of the photon and its direct coupling to quarks, some significant differences to purely hadronic reactions are expected. Since the general features of hadronic minimum bias events are well known, it is convenient to characterize photon-photon interactions comparing to proton-proton and photon-proton interactions. In the following some model predictions for inelastic hadron production in proton-proton, photon-proton and photon-photon collisions are compared at fixed center-of-mass (CMS) energies $\sqrt{s}$. In order to compare to $p\bar{p}$ data, elastic/quasi-elastic scattering (i.e. $\gamma + \gamma \to V + V$, $V = \rho, \omega, \phi$) was excluded in the calculations.

As first discussed by Schuler and Sjöstrand [8, 9], the fraction of hard interactions in minimum bias interactions rises from proton-proton collisions over photon-proton collisions to photon-photon collisions (see Fig. 12.a). The reason for this is the direct photon interaction and the fact, that the photon structure function is considerably harder than the proton structure function. However, these differences in the hard scattering do not

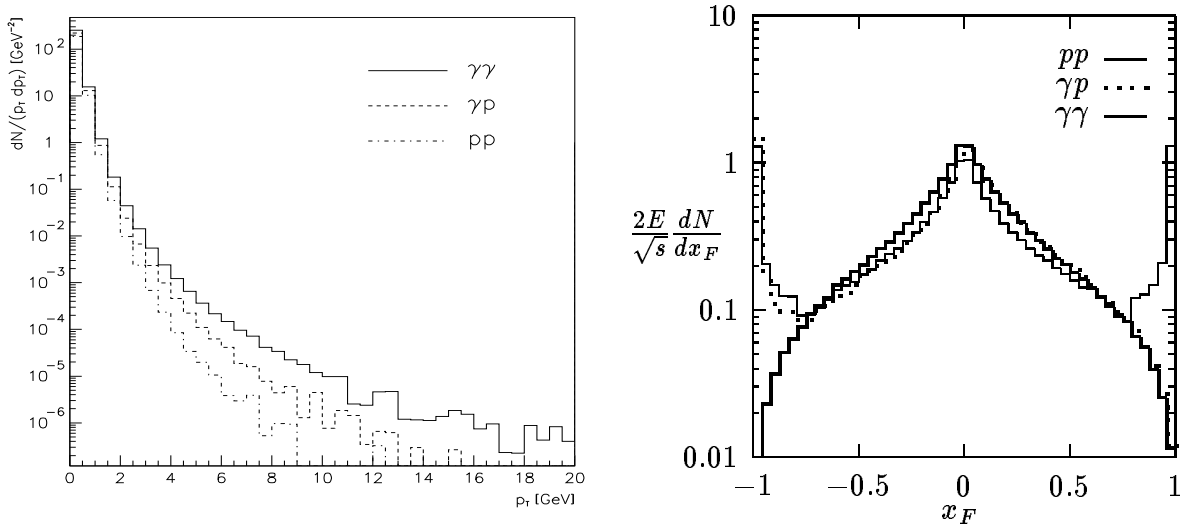

Figure 12: (a) Comparison of the transverse momentum distribution for all charged hadrons produced in proton-proton, photon-proton and photon-photon collisions at $\sqrt{s} = 200$ GeV. The calculation was done with PYTHIA [9]. (b) Invariant form of the x_F distribution for all charged hadrons produced in proton-proton, photon-proton and photon-photon collisions at $\sqrt{s} = 200$ GeV. The calculation was done with PHOJET [11] for inelastic collisions.

strongly influence such average properties of the collision as average multiplicities or even average transverse momenta. This can be seen from Table 3, where we collect some average quantities characterizing nondiffractive collisions. The total and charged multiplicities at all energies are rather similar in all channels. The differences in the multiplicities of hadrons like π^- and $\bar{p}$ are more significant, we find them at all energies rising from pp

Table 1: Comparison of average quantities characterizing hadron production in nondiffractive pp, γp and $\gamma\gamma$ collisions at CMS energies at 50 and 200 GeV [11] The energies are given in GeV and average the transverse momenta are given in GeV/c.

Quantity	pp	γp	$\gamma\gamma$	pp	γp	$\gamma\gamma$
$\sqrt{s}$	50	50	50	200	200	200
$n_{\rm tot}$	24.8	26.5	26.9	40.1	46.2	47.5
$n_{\rm ch}$	14.5	15.5	15.6	23.3	26.9	27.6
n_{π^-}	5.49	6.19	6.53	9.16	10.94	11.46
$n_{\bar{p}}$	0.21	0.27	0.34	0.46	0.59	0.67
$\langle p_\perp \rangle_{\pi^-}$	0.33	0.35	0.40	0.35	0.38	0.42
$\langle p_\perp \rangle_{\bar{p}}$	0.44	0.47	0.57	0.47	0.53	0.64

over γp to $\gamma\gamma$ collisions. Also the average transverse momenta rise in the same way.

In Fig. 12.b we compare the longitudinal momentum distributions in the invariant form for the three channels. Significant differences between the three channels are found in the region near $x_F = 1$ or -1. In pp and γp interactions, the single diffractive component is characterized by leading protons which are obviously missing in $\gamma\gamma$ collisions.

6.3.2 Jet production

Data on jet production in collisions of quasi-real photons have been reported by several experiments (a review is given in [15]). Here, we pick out for comparison the fully acceptance corrected, jet data published by the TOPAZ and AMY Collaborations [16, 17]. These data were already compared to leading [18] and to next-to-leading order QCD calculations in [19],[20]. In Figs. 13.a and 13.b we compare PHOJET [11] results calculated using the GRV LO photon structure function [13] with the data on single jet and two jet transverse momentum distributions [16, 17]. The anti-tag conditions and kinematical cuts of the experiments were applied to the PHOJET events. The jets are searched from the Monte Carlo events on hadron level using a cone jet finding algorithm with the cone radius $R = 1$. The cross sections for these jets, which should approximately correspond to the jets identified in the experiment are compared to the data. To illustrate the difference of these hadron jet cross sections to the cross sections treating each hard parton ($p_\perp > 3$GeV/c) as a single jet, we include in the Figs. also the nonfragmented parton cross sections. There is a systematic difference between the model and the TOPAZ data, the model is below the data. It is interesting, that the calculation of Kleinwort and Kramer [20], which uses the same GRV photon structure functions, shows the same disagreement to the single jet data as found using PHOJET in Fig. 13.a.

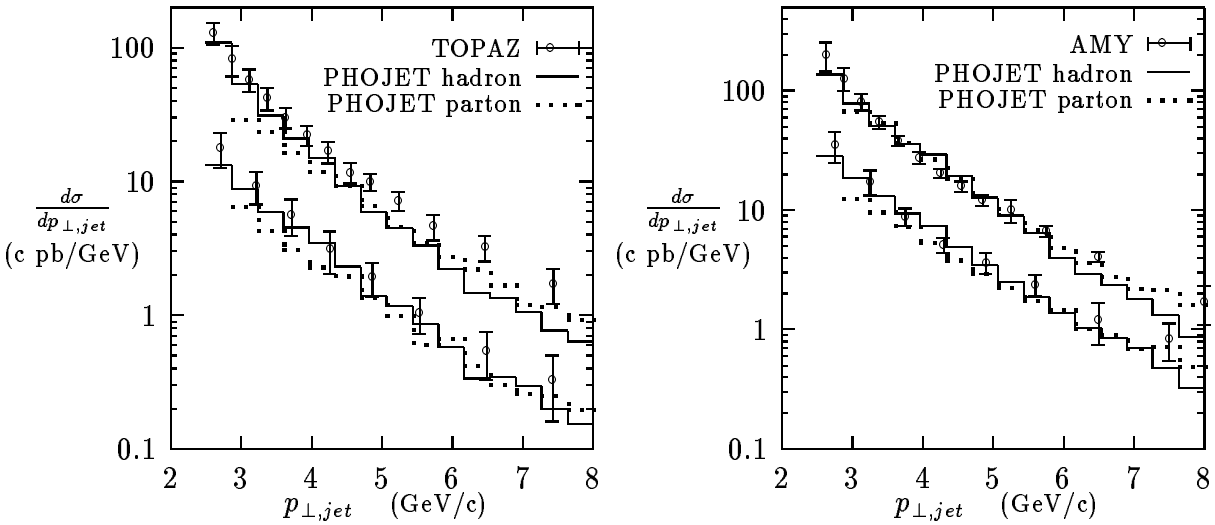

Figure 13: (a) Comparison of single jet $p_\perp$ cross sections (upper curves) and two-jet $p_\perp$ cross sections (lower curves) from [16, 17] with PHOJET [11] results. In addition, the cross section identifying each parton with $p_\perp > 3$ GeV/c with a jet (dottes lines) are shown.

Table 2: Average photon-photon energies and cross sections for the three photon spectra folded with the $\gamma\gamma$ cross section at two linear collider energies. The energies are given in GeV.

$\sqrt{s}_{e^+e^-}$	spectrum	$\sqrt{s}_{\gamma\gamma}$	σ (μb)	$\sqrt{s}_{e^+e^-}$	spectrum	$\sqrt{s}_{\gamma\gamma}$	σ (μb)
500	Bremsst.	50	0.0067	1000	Bremsst.	105	0.0075
500	Beamst.	16.7	0.038	1000	Beamst.	41	0.026
500	B.Laser	252	0.47	1000	B.Laser	509	0.59

6.3.3 Hadron production at Tesla

Two-photon physics at future e^+e^- linear colliders has been discussed by several authors, for example see [21, 3]. These studies are mainly restricted to processes involving large momentum transfers. Here, we consider minimum bias distributions which may be important for background estimatess and detector design. As example, the calculations are done for the TESLA collider design [22].

Using the approximations discussed in Sec. 6.1 we plot in Fig. 14.a the photon spectra according to the equivalent photon approximation, the beamstrahlung spectrum using the bunch parameters [22] as given in the caption of Fig. 14 and a backscattered laser spectrum. The photon virtuality was restricted to $P^2 \leq 2$ GeV^2/c^2. The corresponding photon-photon luminosity functions are shown in in Fig. 14.b. For the calculations, the cut $\sqrt{s}_{\gamma\gamma} > 5$ GeV has been applied. In Table 2 we give the average photon-photon energies and the cross sections for the three processes at two energies. From Fig. 14 and Table 2 we see, that the beamstrahlung spectrum of the TESLA project is the softest of the three photon spectra, the backscattered laser spectrum is the hardest. Of course, in

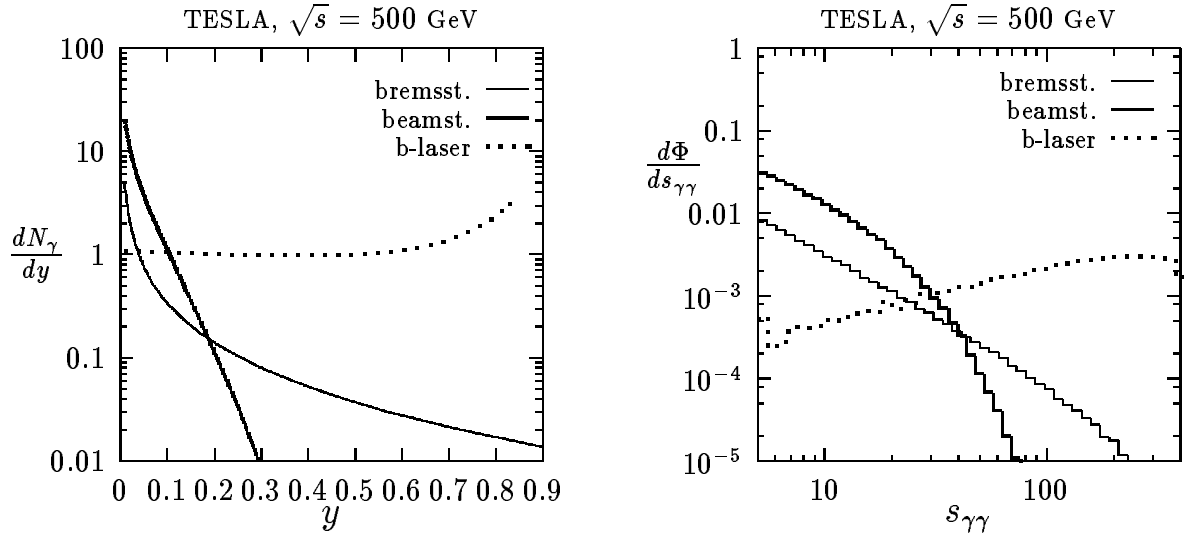

Figure 14: (a) Photon fluxes at a $\sqrt{s} = 500$ GeV linear collider TESLA [22]. Given are the bremsstrahlung spectrum, the beamstrahlung spectrum using the bunch parameters $N_e = 1.8\ 10^{10}$, $\sigma_x = 598$ nm, $\sigma_y = 6.5$ nm and $\sigma_z = 0.5$ mm [22], and a backscattered laser spectrum. (b) photon-photon luminosity function (normalized to the ee luminosity).

the case of a linear collider one has to consider for background problems the superposition of the beamstrahlung spectrum and the bremsstrahlung spectrum.

In Fig. 15.a we plot the cross sections $\sigma dE_\perp/d\eta$ for the transverse energy as function of pseudorapidity for the charged hadron production as function of pseudorapidity. It is clearly visible, that the backscattered laser spectrum is rather hard and has the highest weight. The beamstrahlung spectrum and the bremsstrahlung spectrum are rather comparable, the former has the higher weight, the latter is the harder of these two. The same differences between the three photon spectra are visible in the cross sections $d\sigma/dp_\perp$ for charged hadron production as function of the transverse momentum in Fig. 15.b for the 500 GeV TESLA collider. The $p_\perp$ distributions for the bremsstrahlung spectrum and the beamstrahlung spectrum cross. At low $p_\perp$ the beamstrahlung dominates, at high $p_\perp$ the bremsstrahlung spectrum dominates.

6.3.4 Jet production in semihard processes

We discuss in this section the jet production, inclusive and with rapidity gaps, in the semihard region, $\sqrt{s_{\gamma\gamma}} \gg p_\perp$, with $p_\perp$ the jet transverse energy. In the semihard region a fixed-order perturbative calculation of the jet-production rates may be not sufficient to describe the multiple gluon radiation, and may be necessary to resum the large logarithms, $\ln(s_{\gamma\gamma}/p_\perp^2)$, as is done in the BFKL theory [23]. This predicts that the (enhancement) K-factor of the total parton-parton cross section exhibits a power-like growth in the parton center-of-mass energy $\sqrt{\hat{s}}$. In the case of inclusive two-jet production at large rapidity intervals $\Delta\eta$ between the jets, we obtain $\Delta\eta \simeq \ln(\hat{s}/p_\perp^2)$, and the growth of the K-factor with $\hat{s}$ above mentioned may be read out as the growth of the two-jet K-factor with $\Delta\eta$

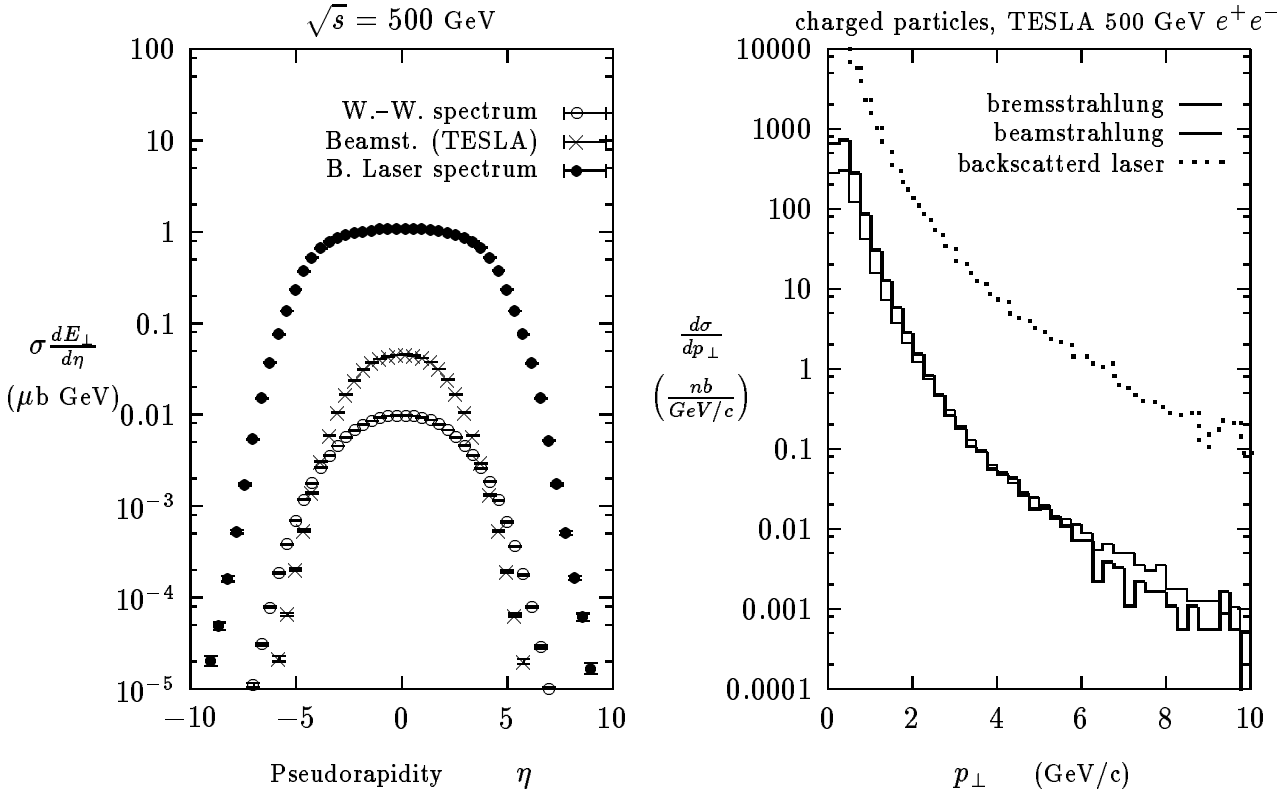

Figure 15: (a) Cross section weighted transverse energy distributions $\sigma dE_\perp/d\eta$ measured in μb GeV at the $\sqrt{s} = 500$ and 1000 GeV TESLA linear colliders [22]. Given are the distributions for the bremsstrahlung photon spectrum, the beamstrahlung spectrum and a backscattered laser spectrum. (b) Transverse momentum cross sections $d\sigma/dp_\perp$ at the $\sqrt{s} = 500$ GeV TESLA linear collider [22]. Given are the distributions for the bremsstrahlung photon spectrum, the beamstrahlung spectrum and a backscattered laser spectrum [11].

[24]. Since $\hat{s} = x_1 x_2 s$, with $x_{1,2}$ the momentum fractions of the incoming partons and $\sqrt{s}$ the hadron center-of-mass energy, $\Delta\eta$ may be increased either by increasing the x's or by increasing s; the former is feasible in a fixed-energy collider, like the Tevatron, but it is not desirable because it introduces a damping in the cross section due to the falling parton luminosity, as $x \to 1$ [25]; the latter is the optimal setting because by fixing the parton densities (up to a residual but mild variation due to $p_\perp$) it looks mainly at the parton dynamics, but it requires a variable-energy collider. An e^+e^- linear collider works like a variable-energy hadron collider if we consider the bremsstrahlung and beamstrahlung spectra for quasi-real photons and ramp the photon-photon center-of-mass energy $\sqrt{s} = \sqrt{s_{\gamma\gamma}}$ up, at fixed parton momentum fractions x/y within the photons. For example, for a 1000 GeV TESLA collider let us consider a brems/beamstrahlung spectrum with photon momentum fractions $0.05 \leq y_1 = y_2 \leq 0.5$, and the production of two jets at $x_1/y_1 = x_2/y_2 = 0.2$. This entails that $10 \leq \sqrt{\hat{s}} \leq 100$ GeV, and for jet transverse momenta $p_\perp \geq 5$ GeV, that $1.4 \leq \Delta\eta \leq 6$.

Analogously, we can treat two-jet production with a large rapidity gap $\Delta\eta_{gap}$ in hadron production between the jets, with $\Delta\eta_{gap} = \Delta\eta - 2R$ and $\Delta\eta$ the rapidity interval between the jet centers and R the jet-cone size. The absence of gluon radiation between the jets

may be modeled as due to the exchange of a colorless object, with momentum transfer $t \simeq -p_\perp^2$. The probability that this is due to one-gluon exchange falls exponentially with $\Delta\eta$, while the probability of it being due to two-gluon exchange in a colorless combination, i.e. to a perturbative pomeron, is in a first approximation independent of $\Delta\eta$ [26], [27], [28]. However, if the colliding particles are hadrons, or hadron-like, the additional soft interactions between the spectator partons may fill in the gap with soft hadrons [26]. A way of avoiding it is to require that at least one of the colliding particles is point-like, namely in $\gamma\gamma$ collisions that one of the photons is off shell. Thus we consider two-jet production in $\gamma^*\gamma$ DIS events, with one jet in the current fragmentation region, the *current jet*, and the other close to the γ fragmentation region, the *forward jet*. To minimize the variation of the parton densities we require as in the inclusive case that the parton momentum fraction x/y within the photon γ is fixed [28]. However we may ramp the off-shell-photon/parton center-of-mass energy $\hat{s}_{\gamma^* p}$ up even at fixed γ-beam energies by decreasing x_{bj}, since $\Delta\eta \simeq \ln(\hat{s}_{\gamma^* p}/Q^2) = \ln(x/y x_{bj})$. In order to maximize the energy we may run the γ beam in the backscattered laser mode, which entails that $s_{e\gamma} \simeq 8 \cdot 10^5\, GeV^2$. Thus for an electron scattered at $\theta \simeq 12.6$ mrad we have $Q^2 \simeq 40\, GeV^2$, and for a realistic electron energy loss $y_e \simeq 0.25$ we find $x_{bj} \simeq 2 \cdot 10^{-4}$. So for $x/y = 0.2$, we obtain $\Delta\eta \simeq 6.9$, which for a jet-cone size $R = 1$ yields gaps of size $\Delta\eta_{gap} \simeq 5$, which is about the size required to make this study relevant [29].

The study of the perturbative Pomeron can also be done using the quasidiffractive channels of type

$$\gamma\gamma \to M\ M', \qquad\qquad \gamma\gamma \to M + X \tag{28}$$

in the semihard region

$$s \gg p_\perp^2 = |t| \gg \mu^2, \quad t = (p_{1\gamma} - p_M)^2, \quad \mu = 0.3\,\mathrm{GeV}. \tag{29}$$

Here M is a vector ($V = \rho^0, \omega, \phi, ...\Psi$), or pseudovector ($P = \pi^0, \eta, \eta'$), or tensor ($T = a_2, f_2, f'$) neutral meson and X is a hadron system with not too large invariant mass $M_X^2 \lesssim |t|$. Such processes are discussed in a number of papers [30, 31, 32]. The same enhancement K-factor as discussed above holds also for these processes which may lead to a large production rate already at LEP2 [33]. These processes certainly deserve further investigations at the linear colliders.

6.3.5 Jet production in hard processes

We turn now to inclusive jet production, without rapidity gaps, at large enough transverse momenta so that the usual perturbative QCD framework applies. Precision phenomenology requires next-to-leading order (NLO) calculations [19],[20]. Jet production studies are well known to complement the deep-inelastic structure function studies (see sec. 4) as they are sensitive to the gluon content of the photon which is poorly constrained the structure function data.

In the following we discuss jet production in a e^+e^- collider at 500 GeV and, for the purpose of the discussion, we consider only bremsstrahlung-bremsstrahlung and beamstrahlung-

beamstrahlung collisions. In the former case, the spectrum eq. (22) is used with the constraints $y < .5$ and $\Theta_{max} = 175$ mrad (no detector inside the shielding mask is assumed). As indicated in Fig. 15.b, the bremsstrahlung process dominates at large transverse momentum: we find that it is an order of magnitude larger than the beamstrahlung induced one at $p_T = 30$ GeV/c. Also to be noted is the high rate of jet production: for an integrated luminosity of 20 fb^{-1} we expect about 100 events/GeV/c at $p_T^{jet} = 55$ GeV/c in the pseudo-rapidity interval $-.5 < \eta < .5$. The rapidity distribution of jets with $p_T > 15$ GeV/c is shown in Fig. 16.a: the bremsstrahlung photons being much harder than the beamstrahlung ones (see Fig. 14) the jet rapidity distribution extends over a much wider domain in the former case. The various components of the cross section are displayed in

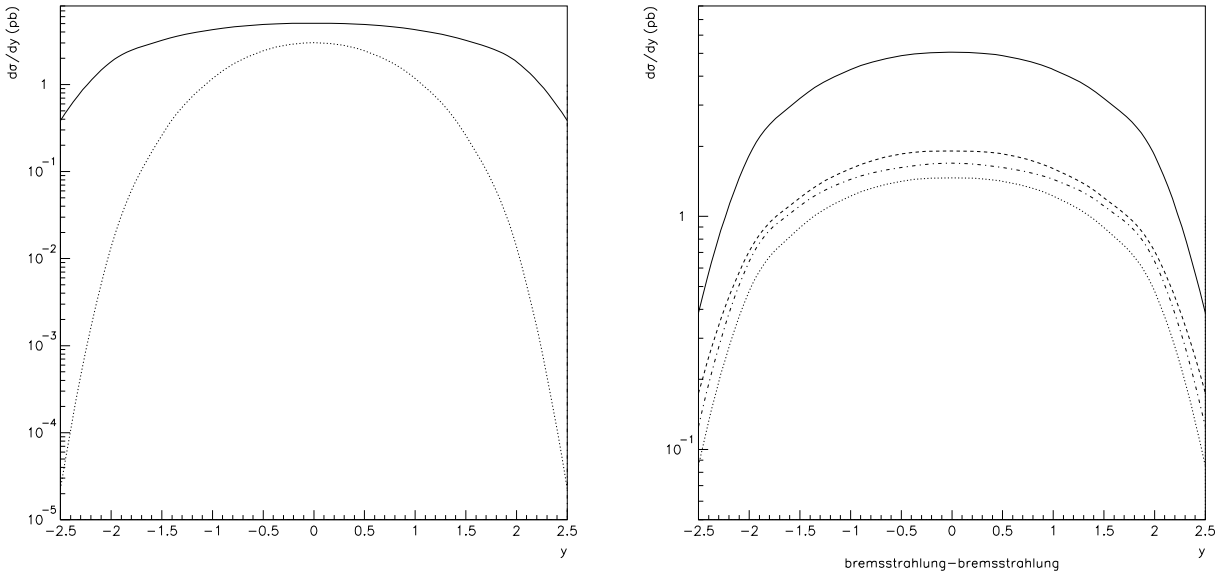

Figure 16: (a) Jet pseudo-rapidity distribution for $p_T > 15$ GeV/c: bremsstrahlung-bremsstrahlung scattering (solid line) and beamstrahlung-beamstrahlung scattering (dashed line). (b) Details of the pseudo-rapidity distribution: full cross section (solid line), direct term (dashed line), one-resolved (dotted line) and two-resolved (dash-dotted line)

Fig. 16.b: all components are rougly similar in size with the "direct" one (both photons couple directly to the hard sub-process) being the largest and the one-resolved one (one photon interacts via its quark or gluon content) being the smallest. Such a hierarchy between the various pieces depend crucially on the shape of the incoming photon spectrum: indeed, in the beamstrahlung process, the double-resolved component becomes considerably suppressed (one order of magnitude smaller) compared to the dominant direct one. This is explained by the rapidly falling parton-parton luminosity for beamstrahlung scattering. In reference to the photon structure let us mention that, even at high energies, the non-perturbative (sometimes called the VDM or hadronic) component plays a non negligible role. For example, for a jet p_T value of 10 GeV/c (corresponding to a hard (scale)$^2 \simeq 100$ GeV^2) one can estimate the VDM component in the photon to still account for about 25% of the cross section: although the non-perturbative component is, a priori, not expected to be so important at large scales, the reason for this is the fact that the

effective x values probed in this process are rather small, and, the smaller the x value is, the larger is the hadronic component (see sec. 4).

All the above is based on leading-order (LO) calculations. The NLO corrections, globally, do not play an important role. For instance studying, at fixed $p_T = 15$ GeV/c and $\eta = 0$, the cross section dependence as a function of the opening "angle" R of the jet we find (all arbitrary scales set equal to p_T), in pb/GeV/c, $d\sigma/dp_T/d\eta = 1.00,\ 1.13$ and 1.24 for $R = .4,\ .7$ and 1. respectively to be compared to $d\sigma/dp_T/d\eta = 1.08$ (obviously independent of R) in the LO approximation. From the theoretical point-of-view, the main advantage of the higher-order calculation is a much improved stability of the predictions under changes of the arbitrary scales [19]. On the phenomenological side, it should be known that the smallness of the corrections to the inclusive jet production hides large compensating corrections to the various components as discussed in the LEP2 report [33]. The direct component is decreased (by about 15%) and the double-resolved one is increased by as much as 40% while the one-resolved component remains stable. We conclude that the overall structure of the events is rather affected by the higher-order corrections.

We emphasized above single-jet phenomenology. Using the very recent NLO calculations for di-jet production [20] much precise phenomenology can now be done using this observable. Following HERA studies [34] one could use the di-jet (or the multi-jet) configurations to calculate the fractions x_1, x_2 of parton momenta in the photons from experimental variables and relate directly the shape of the parton distributions to experimental observables [35].

Acknowledgements

This research is supported in part by the EEC program "Human Capital and Mobility", Network "Physics at High Energy Colliders", contract CHRX-CT93-0357 (DG 12 COMA).

References

[1] V. M. Budnev, I. F. Ginzburg, G. V. Meledin and V. G. Serbo: Phys. Rep. 15C (1975) 181

[2] P. Chen: Phys. Rev. D46 (1992) 1186

[3] P. Chen, T. L. Barklow and M. E. Peskin: Phys. Rev. D49 (1994) 3209

[4] D. Schulte, previous section. The parameters used here were the TESLA values in Summer 1995.

[5] I. F. Ginzburg, G. L. Kotkin, V. G. Serbo and V. I. Telnov: Prisma ZHETF 34 (1981) 514; Nucl. Instrum. Methods A205 (1983) 47

[6] I. F. Ginzburg, G. L. Kotkin, S. L. Panfil, V. G. Serbo and V. I. Telnov: Nucl. Instrum. Methods A219 (1984) 5

[7] V. I. Telnov: Nucl. Instrum. Methods A294 (1990) 72

[8] G. A. Schuler and T. Sjöstrand: Nucl. Phys. B407 (1993) 539
[9] G. A. Schuler and T. Sjöstrand: $\gamma\gamma$ and γp events at high energies, CERN-TH.7193/94, presented at the Workshop on Two-Photon Physics, Paris, 1994
[10] R. Engel: Z. Phys. C66 (1995) 203
[11] R. Engel and J. Ranft: Hadronic photon-photon collisions at high energies, ENSLAPP-A-540/95 (hep-ph/9509373)
[12] C. Corsetti, R. M. Godbole and G. Pancheri: see the following section
[13] M. Glück, E. Reya and A. Vogt: Phys. Rev. D46 (1992) 1973
[14] G. A. Schuler and T. Sjöstrand: Low- and high-mass components of the photon distribution functions, CERN-TH/95-62
[15] D. Morgan, M. R. Pennington and M. R. Whalley: J. Phys. G 20 (1994) A1
[16] TOPAZ Collab.: H. Hayashii et al.: Phys. Lett. B314 (1993) 149
[17] AMY Collab.: B. J. Kim et al.: Phys. Lett. B325 (1994) 248
[18] M. Drees and R.M. Godbole, J. Phys. **G21** (1995) 1559
[19] P. Aurenche, J. P. Guillet, M. Fontannaz, Y. Shimizu and K. Kato: Prog. Theor. Phys. 92 (1994) 175
[20] T. Kleinwort and G. Kramer: Inclusive one and two-jet cross sections in $\gamma\gamma$-processes at e^+e^- colliders, DESY 96-035
[21] M. Drees and R. M. Godbole: Z. Phys. C59 (1993) 591
[22] R. Brinkmann: SBLC and TESLA general design overview, Presentation at the Linear Collider workshop, Gran Sasso, Italy, 1995
[23] L.N. Lipatov in "*Perturbative QCD*" A.H. Mueller ed., World Scientific 1989, and references therein
[24] A.H. Mueller and H. Navelet: Nucl. Phys. B282 (1987) 727
[25] V. Del Duca and C.R. Schmidt: Phys. Rev. D49 (1994) 4510;
W.J. Stirling: Nucl. Phys. B423 (1994) 56
[26] J.D. Bjorken: Phys. Rev. D47 (1992) 101
[27] A.H. Mueller and W.-K. Tang: Phys. Lett. B284 (1992) 123
[28] V. Del Duca and W.-K. Tang: Phys. Lett. B312 (1993) 225;
Proceedings of the 5^{th} Blois Workshop on Elastic and Diffractive Scattering (1993), ed. H.M. Fried et al., World Scientific 1994
[29] S. Abachi et al. (D0 Collaboration): Phys. Rev. Lett. 72 (1994) 2332;
F. Abe et al. (CDF Collaboration): Phys. Rev. Lett. 74 (1995) 855
[30] V.L. Chernyak and A.R. Zhitnitsky, Nucl. Phys. **B222** (1983) 382; Phys. Rep. **112** (1984) 173; I.F. Ginzburg, D.Yu. Ivanov, V.G. Serbo, Sov.Yad.Fiz. **56** (1993) 45
[31] I.F. Ginzburg, S.L. Panfil, V.G. Serbo, Nucl.Phys. **B284** (1987) 685; I.F. Ginzburg, D.Yu. Ivanov, Nucl. Phys. B (Suppl.) **25B** (1992) 224; Nucl.Phys. **B388** (1992) 376
[32] J.R.Forshaw and M.G.Ryskin, Z.Phys. **C68** (1995) 137
[33] $\gamma\gamma$ physics, P. Aurenche and G.A. Schuler convenors, in CERN Yellow report, CERN 96-01
[34] T. Ahmed, H1 collaboration, Nucl. Phys. **B445** (1995) 195;
M. Derrick, ZEUS collaboration, Phys. Lett. **B348** (1995) 665
[35] $\gamma\gamma$ generators, L. Lönnblad and M. Seymour convenors, in CERN Yellow report, CERN 96-01

7 Eikonalized mini-jet cross-Sections

A. Corsetti[1], R.M. Godbole[2], G. Pancheri[3]

[1] *INFN, Univ. La Sapienza, Roma, Italy* [2] *CTS, IIS, Bangalore, India*
[3] *INFN, Frascati, Italy*

In this note we wish to assess the validity and uncertainties of the eikonalized mini-jet model in predicting $\sigma_{\gamma\gamma}^{inel}$ and further to ascertain whether measurements at LEP-200 and HERA can constrain various parameters of the model. In its simplest formulation, the eikonalized mini–jet cross-section is given by

$$\sigma_{ab}^{inel} = P_{ab}^{had} \int d^2\vec{b}[1 - e^{-n(b,s)}] \tag{30}$$

where the average number of collisions at a given impact parameter $\vec{b}$ is obtained from

$$n(b,s) = A_{ab}(b)(\sigma_{ab}^{soft} + \frac{1}{P_{ab}^{had}}\sigma_{ab}^{jet}) \tag{31}$$

with $A_{ab}(b)$ the normalized transverse overlap of the partons in the two projectiles and P_{ab}^{had} to give the probability that both colliding particles a, b be in a hadronic state. σ_{ab}^{soft} is the non-perturbative part of the cross-section from which the factor of P_{ab}^{had} has already been factored out and σ_{ab}^{jet} is the hard part of the cross–section. The rise in σ_{ab}^{jet} drives the rise of σ_{ab}^{inel} with energy [1]. We have also assumed the factorization property

$$P_{\gamma p}^{had} = P_{\gamma}^{had}; \quad P_{\gamma\gamma}^{had} = (P_{\gamma}^{had})^2.$$

The predictions of the eikonalised mini-jet model [2] for photon induced processes [3] depend on 1) the assumption of one or more eikonals, 2) the hard jet cross-section $\sigma_{ab}^{jet} = \int_{p_{tmin}} \frac{d^2\hat{\sigma}}{dp_t^2} dp_t^2$ which in turn depends on the minimum p_t above which one can expect perturbative QCD to hold, viz. p_{tmin}, and the parton densities in the colliding particles a and b, 3) the soft cross–section σ_{ab}^{soft}, 4) the overlap function $A_{ab}(b)$, defined as

$$A_{ab}(b) = \frac{1}{(2\pi)^2} \int d^2\vec{q}\mathcal{F}_a(q)\mathcal{F}_b(q)e^{i\vec{q}\cdot\vec{b}} \tag{32}$$

where $\mathcal{F}$ is the Fourier transform of the b-distribution of partons in the colliding particles and 5) last but not the least P_{ab}^{had}.

In this note we shall restrict ourselves to a single eikonal. The hard jet cross-sections have been evaluated in LO perturbative QCD. The dependence of σ_{ab}^{jet} on p_{tmin} is strongly correlated with the parton densities used. Here we show the results using GRV densities [4] (see ref. [5] for the results using the DG densities [6]). For the purposes of this note, we determine $\sigma_{\gamma\gamma}^{soft}$ from $\sigma_{\gamma p}^{soft}$ which is obtained by a fit to the photoproduction data. We use the Quark Parton Model suggestion $\sigma_{\gamma\gamma}^{soft} = \frac{2}{3}\sigma_{\gamma p}^{soft}$.

In the original use of the eikonal model, the overlap function $A_{ab}(b)$ of eq. (32) is obtained using for $\mathcal{F}$ the electromagnetic form factors and thus, for photons, a number of authors [7, 8] have assumed for $\mathcal{F}$ the pole expression used for the pion electromagnetic form factor, on the basis of Vector Meson Dominance (VMD). We shall investigate here another possibility, i.e. that the b-space distribution of partons in the photon is the Fourier transform of their intrinsic transverse momentum distributions. This will correspond to use the functional expression expected for the perturbative part [9]

$$\frac{dN_\gamma}{dk_t^2} = \frac{1}{k_t^2 + k_o^2} \tag{33}$$

Recently this expression was confirmed by the ZEUS [10] Collaboration, with $k_o = 0.66 \pm 0.22$ GeV. For $\gamma\gamma$ collisions, the overlap function is now simply given by

$$A(b) = \frac{1}{4\pi} k_o^3 b K_1(bk_o) \tag{34}$$

with K_1 the Bessel function of the third kind. It is interesting to notice that for photon-photon collisions the overlap function will have the same analytic expression for both our ansätze: the VMD inspired pion form factor or the intrinsic transverse momentum; the only difference being that the former corresponds to a fixed value of $k_0 = 0.735$ GeV whereas the latter allows us to vary the value of the parameter k_0. Thus both possibilities can be easily studied by simply changing k_0 appropriately. Notice that the region most important to this calculation is for large values of the parameter b, where the overlap function changes trend, and is larger for smaller k_o values.

As for P_γ^{had}, this is clearly expected to be $\mathcal{O}(\alpha_{em})$ and from VMD one would expect 1/250. From phenomenological considerations [8]and fits to HERA data, one finds a value 1/200, which indicates at these energies a non-VMD component of $\approx 20\%$. It should be noticed that the eikonalised minijet cross–sections do not depend on $A_{\gamma\gamma}$ and $P_{\gamma\gamma}^{had}$ separately, but depend only on the ratio of the two [11, 12].

Having thus established the range of variability of the quantities involved in the calculation of total photonic cross sections, we now proceed to calculate and compare with existing data the eikonalized minijet cross-section for $\gamma\gamma$ collisions. We use GRV (LO) densities and values of p_{tmin} deduced from a best fit to photoproduction. As discussed in [15], it is possible to include the high energy points in photoproduction using GRV densities and $p_{tmin} = 2$ GeV, but the low energy region would be better described by a smaller p_{tmin}. This is the region where the rise, according to some authors, notably within the framework of the Dual Parton Model, is attributed to the so-called *soft Pomeron*. For our studies here we use $p_{tmin} = 2.$ GeV. We also use $P_\gamma^{had} = 1/204$ and A(b) from eq.(34) with different values of k_0. One choice for k_0 is the pole parameter value in the photon b-distribution expression, which includes both the intrinsic transverse momentum option 0.66 ± 0.22 GeV as well as the pion form factor value, 0.735 GeV. The other value, 1 GeV, is a possible choice which appears to fit the present data better than everything else. Our predictions are shown in Fig.(17). A comparison with existing $\gamma\gamma$ data shows that all of our choices are compatible with the data within the present experimental errors. At high energies, however, like the ones reachable with the proposed linear photon colliders, these

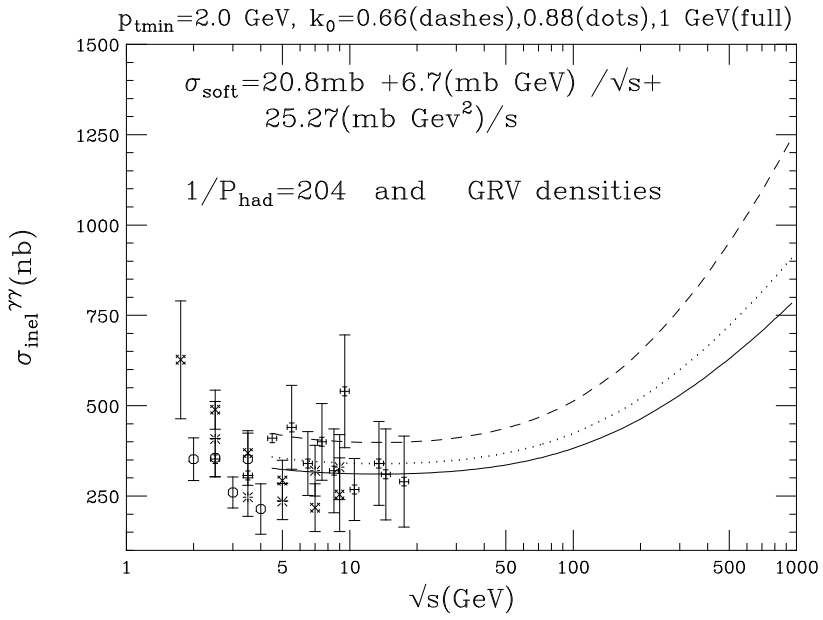

Figure 17: Total inelastic photon-photon cross-section for $p_{tmin} = 2.$ GeV and different parton b-distribution in the photon. The solid line corresponds to $k_0 = 1.$ GeV.

predictions vary by about $\pm 25\%$. Reducing the error in the LEP1 region and adding new data points in the c.m. region attainable at LEP2, can help pinpoint and restrict the choices. Were the LEP1 and LEP2 data to confirm the present values, we believe that the best representation of the present data is obtained with the higher k_0 value.

Acknowledgements

R.M.G. wishes to acknowledge support from C.S.I.R. (India) under grant no. 03(0745)/94/EMR-II. This research is supported in part by the EEC program "Human Capital and Mobility", contract CT92-0026 (DG 12 COMA).

References

[1] D.Cline et al., Phys. Rev. Lett. **31** (1973) 491, T.Gaisser and F.Halzen, Phys. Rev. Lett. **54** (1985) 1754, G.Pancheri and Y.N.Srivastava, Phys. Lett. **B182** (1985).

[2] A. Capella and J. Tran Thanh Van, Z. Phys. **C23** (1984)168, P. l'Heureux, B. Margolis and P. Valin, Phys. Rev. **D 32** (1985) 1681, L. Durand and H. Pi, Phys. Rev. Lett. **58** (1987) 58.

[3] J.C. Collins and G.A. Ladinsky, Phys. Rev. **D 43** (1991) 2847.

[4] M. Glück, E. Reya and A. Vogt, Phys. Rev. **D 46** (1992) 1973.

[5] M. Drees and R.M. Godbole, Z. Phys. **C 59** (1993) 591.

[6] M. Drees and K. Grassie, Z. Phys. **C28** (1985) 451.

[7] K. Honjo et al., Phys. Rev. **D 48** (1993) 1048.

[8] R.S. Fletcher, T.K. Gaisser and F.Halzen, Phys. Rev. **D 45** (1992) 377; erratum Phys. Rev. **D 45** (1992) 3279.

[9] J. Field, E. Pietarinen and K. Kajantie, Nucl. Phys. **B 171** (1980) 377; M. Drees, *In the proceedings of the 23rd International Symposium on Multiparticle Dynamics, Aspen, Colo., Sep. 1993, Eds. M.M. Block and A.R. White.*

[10] M. Derrick et al., ZEUS Collaboration , Phys. Lett. **B 354** (1995) 163.

[11] M. Drees, Univ. Wisconsin report MADPH-95-867, *proceedings of the 4th workshop on TRISTAN physics at High Luminosities*, KEK, Tsukuba, Japan, Nov. 1994.

[12] M. Drees and R.M. Godbole, Journal Phys. G., **G 21** (1995) 1559.

[13] H. Abramowicz, K. Charchula and A. Levy, Phys. Lett. **B 269** (1991) 458.

[14] K. Hagiwara, M. Tanaka, I. Watanabe and T. Izubuchi, Phys. Rev. **D51** (1995) 3197.

[15] C. Corsetti, R.M. Godbole and G. Pancheri, in preparation.

8 Heavy flavor production

M. Cacciari[1], R.M. Godbole[2], M. Greco[3], M. Krämer[1], E. Laenen[4], S. Riemersma[5]

[1] *DESY, Hamburg, Germany*
[2] *CTS, IISc, Bangalore, India*
[3] *Roma III and LNF, Italy*
[4] *CERN, Geneva, Switzerland*
[5] *DESY, Zeuthen, Germany*

The production of heavy flavours in two-photon collisions provides an important tool to study the dynamics of perturbative QCD. The mass of the heavy quark, $m_Q \gg \Lambda_{QCD}$, sets the hard scale for the perturbative analysis and ensures that the separation into direct and resolved processes is unambiguous through next-to-leading order (NLO). Hence production via the direct channel is directly calculable in perturbative QCD (pQCD) and in principle the best way for confronting the pQCD prediction with experiment. Resolved processes, on the other hand, provide a good opportunity to measure the poorly known gluon content of the photon. Experimentally one may separate direct and resolved channels by analyzing deep-inelastic $e\gamma$ scattering, by using non-diffractively produced J/ψ's, or by detecting the photon remnant jet, present in the resolved processes only.

Charm quark production in two-photon collisions has been analysed at the e^+e^- colliders PETRA, PEP, TRISTAN and LEP. The experimental status and prospects for LEP2 have been reviewed in Ref. [1]. The high-statistics data to be expected at the NLC will allow for a detailed comparison of the pQCD predictions with experimental results not only for production rates, but also for various differential distributions. These analyses will yield information on the dynamics of heavy flavour production in a kinematical range very different from that available in $\gamma\gamma$ collisions at present colliders.

In the following we will discuss the theoretical predictions for open heavy flavour production in two-photon collisions and in deep-inelastic $e\gamma$ scattering and briefly mention $\gamma\gamma$ production of quarkonia.

8.1 Heavy flavour production in $\gamma\gamma$ collisions

Three mechanisms contribute to the production of heavy quarks in $\gamma\gamma$ collisions. (i) In the case of direct production, the photons couple directly to the heavy quarks. No spectator particles travel along the γ axes. (ii) If one of the photons first splits into a flux of light quarks and gluons, one of the gluons may fuse with the second photon to form the $Q\overline{Q}$ pair. The remaining light quarks and gluons build up a spectator jet in the split γ direction (single resolved γ contribution). (iii) If both photons split into quarks and gluons, the $Q\overline{Q}$ pair is accompanied by two spectator jets (double resolved γ contribution). It turns out *a posteriori* that the double resolved γ contribution is much smaller than the direct and the single resolved γ contributions.

Total cross sections and various distributions for charm and bottom quark production $e^+e^- \to e^+e^-c/bX$ have been calculated in Ref. [2] including QCD radiative corrections for

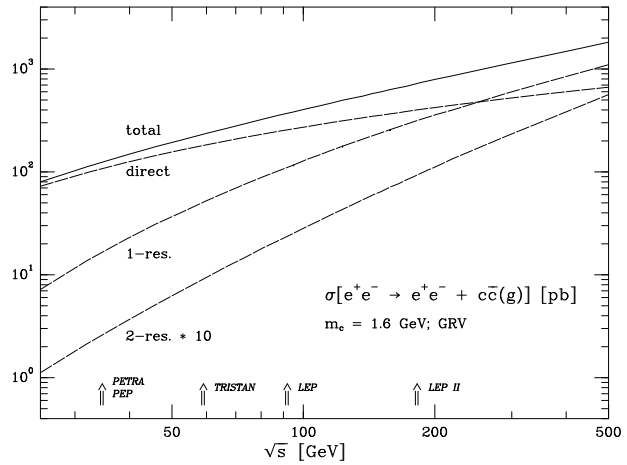

Figure 18: Total cross sections for $e^+e^- \to e^+e^- + c\bar{c}X$ as functions of the e^+e^- collider energy. Parameters as described in Ref. [2].

the leading subprocesses. The energy dependence of the total charm cross section is shown in Fig.18. At low energies in the PETRA/PEP/TRISTAN range, the direct production mechanism is completely dominant, however at LEP2 and higher energies $\gamma\gamma$ production of charm quarks receives contributions in about equal amounts from the direct and single resolved channels. A measurement of the gluon content of the photon, which is currently poorly known, might thus be feasible at LEP2 and the NLC. The agreement between the next-to-leading order predictions [2] and the recent data from PETRA, PEP, TRISTAN and LEP is quite satisfactory [1], even though the experimental errors (statistical and systematic) are large.

At the NLC the higher cms energy and large luminosity will lead to fairly copious production of heavy quark pairs in two-photon collisions [3, 4]. In Table 3 we list the total cross sections $e^+e^- \to e^+e^-c\bar{c}X$ at $\sqrt{s} = 500$ GeV for various input parameters at next-to-leading order accuracy. To compute α_s we used the two loop expression with $\Lambda^{(5)}_{\rm QCD} = 0.215$ GeV and $n_{\rm lf} = 3$ active flavours. The open $c\bar{c}$ threshold energy is set to 3.8 GeV, and the GRV parametrization [5] has been adopted for the quark and gluon densities of the photon. We used the Weizsäcker-Williams density of [6] with an anti-tag angle $\theta_{\rm max}$ of 175 mrad. Beamstrahlung is expected to play an important rôle at a future linear collider, so we include its effect here by adopting for its spectrum the expression given in [7], with parameters $\Upsilon_{\rm eff} = 0.039$ and $\sigma_z = 0.5$ mm [8] corresponding to the TESLA design. We will as default coherently superimpose the Weizsäcker-Williams density and the beamstrahlung density, in order to incorporate the case where one photon is of beam- and the other of bremsstrahlung origin.

The cross sections for charmed particle production are very large, giving a total of $\sim 10^8$ events for an integrated luminosity of $\int\mathcal{L} = 20\,{\rm fb}^{-1}$. Beamstrahlung effects are quite important and increase the cross section significantly, by about a factor five. Other beamstrahlung spectra do not change the total rate too much, e.g. by a factor 1.7 for the JCL spectrum. The production of b quarks is suppressed by factor of ~ 200 as compared to charm, a consequence of the smaller bottom electric charge and the phase

space reduction by the large b mass. From the numbers collected in Table 3 we can conclude that the predictions of the cross sections appear to be theoretically firm. A variation of the charm quark mass m_c and the renormalization/factorization scale μ in the range 1.3 GeV $< \mu < 2\,m_c$ and 1.3 GeV $< m_c <$ 1.7 GeV leads to a total theoretical uncertainty of about $\pm$ 30 %. In order to extract the charm signal it might be necessary to impose stringent cuts. Requiring one of the heavy quarks to have rapidity $|y| \leq 1.7$ and transverse momentum $p_\perp \geq 5$ GeV reduces the charm quark cross section by about a factor of 50 and the b cross section by about a factor three. If one demands the event to contain at least one muon with rapidity $|y| \leq 2$ and $p_\perp(\mu) \geq 5$ GeV for charm tagging, the total $c\bar{c}$ cross section is reduced by at least a factor of 2000 [3]. The muon tagging also reduces the contribution from resolved processes to the signal and hence the sensitivity to the gluon content of the photon. For further details we refer to Ref. [1] where the experimental methods for charm tagging in $\gamma\gamma$ collisions have been reviewed.

Given the large statistics at the NLC it will become possible to measure both heavy quarks and analyse their correlations. The study of these correlations has been performed in Ref. [9] and constitutes a more comprehensive test of the theory. To eliminate the uncertainties related to the parton densities in the photon, the authors of Ref. [9] have concentrated on the direct channel, which is in principle the best channel for confronting the pQCD prediction with experiment. A complete analysis including resolved contributions is in preparation [10]. As an example, we show in Fig. 19 the ΔR distribution, defined by $\Delta R = \sqrt{(\Delta\phi)^2 + (\Delta\eta)^2}$, at LO and NLO for both LEP2 and the NLC in the direct channel. Here $\Delta\phi$ is the azimuthal angle between the charm and anticharm in the

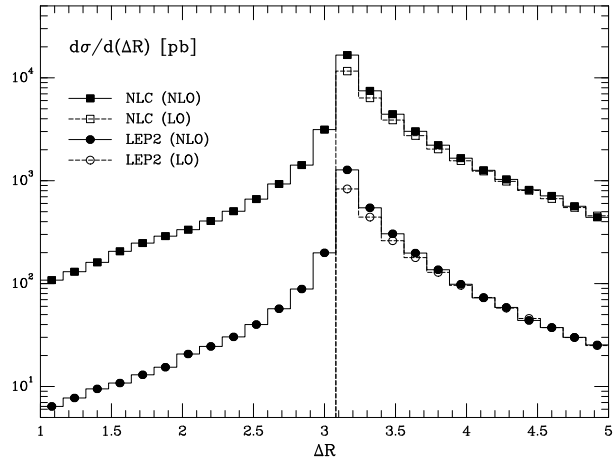

Figure 19: ΔR distribution for charm and anti-charm quark at LEP2 and NLC.

plane transverse to the beam axis and $\Delta\eta$ is the pseudo-rapidity difference of the two heavy quarks. At LO $\Delta R > \pi$, but at NLO ΔR may also assume values below that. It has been demonstrated in Ref. [9] that NLO corrections significantly modify the shapes and normalizations of various distributions and correlations.

In next-to-leading order potentially large terms $\sim \alpha_s \ln(p_\perp/m_Q)$ arise from collinear emission of gluons by a heavy quark at large transverse momentum or from almost collinear branching of gluons or photons into heavy quark pairs. These terms are not

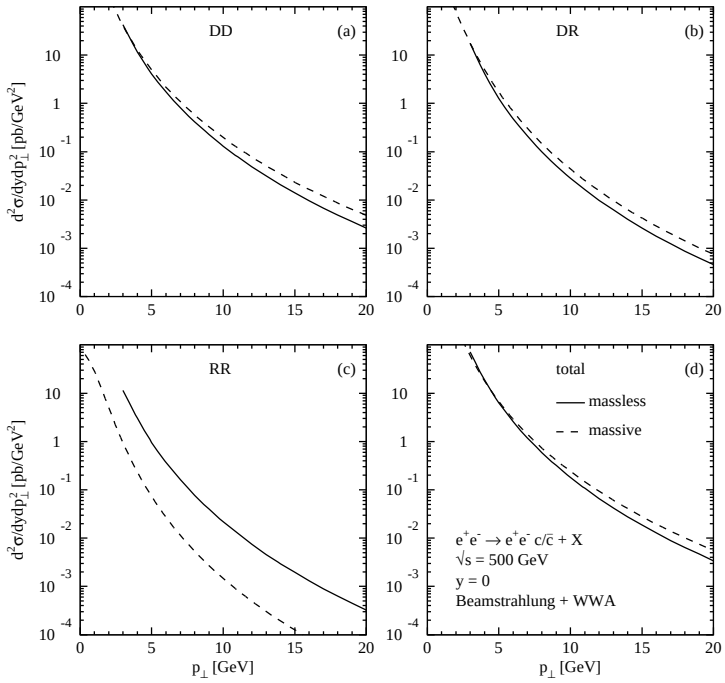

Figure 20: Inclusive cross section $\mathrm{d}^2\sigma/\mathrm{d}y\,\mathrm{d}p_\perp^2$ for $\gamma\gamma$ production of charm quarks as a function of $p_\perp$ for rapidity $y = 0$ in the massless (solid lines) and massive (dashed lines) schemes: (a) direct (DD), (b) single-resolved (DR), (c) double-resolved (RR), and (d) total sum.

expected to affect the total production rates, but they might spoil the convergence of the perturbation series at $p_\perp \gg m_Q$. An alternative way for making predictions at large $p_\perp$ is to treat the heavy quarks as massless partons. The mass singularities of the form $\ln(p_\perp/m_Q)$ are then absorbed into structure and fragmentation functions in the same way as for the light u, d, s quarks. In Ref. [11] the NLO cross section for large $p_\perp$ production of heavy quarks in direct and resolved channels has been calculated in the framework of perturbative fragmentation functions (PFF's) [12]. In Fig. 20 we show the direct (DD), single-resolved (DR) and double resolved (RR) contributions to the differential cross section $\mathrm{d}^2\sigma/\mathrm{d}y\,\mathrm{d}p_\perp^2$ as a function of $p_\perp$ for rapidity $y = 0$ and their sum, respectively, both in fixed-order perturbation theory ("massive") and in the PFF approach ("massless"). The two approaches differ in the definitions and relative contributions of the direct and resolved terms, but essentially agree in their sum. The resummation of the $\alpha_s \ln(p_\perp^2/m^2)$ terms in the PFF approach leads to a softer $p_\perp$ distribution and to a reduced sensitivity to the choice of the renormalization and factorization scales [11]. Similar results have also been obtained in the context of photon-proton collisions in [13].

8.2 Heavy flavour production in deep-inelastic $e\gamma$ scattering

The production of heavy quarks via deep-inelastic $e\gamma$ scattering, i.e. the reaction

$$e^-(p_e) + e^+ \to e^-(p_e') + e^+ + Q(p_1) + X\,, \tag{35}$$

(here we assume the electron to be tagged) proceeds via the subprocess $\gamma^*(q) + \gamma(k) \to Q(p_1) + X$, where one of the photons is highly virtual and the other one is almost on-mass-shell and transversely polarized. $Q(p_1)$ is a heavy quark with momentum p_1 and X denotes any hadronic state allowed by quantum-number conservation. The cross section of this process can be expressed in terms of structure functions:

$$\frac{d^2\sigma}{dx dQ^2} = \int dz\, f_\gamma^e(z, \frac{S}{m_e^2})\, \frac{2\pi\alpha^2}{x\, Q^4} \left[(1 + (1-y)^2) F_2^\gamma(x, Q^2, m^2) - y^2 F_L^\gamma(x, Q^2, m^2)\right] . \quad (36)$$

Here m is the heavy quark mass, z the momentum fraction of the target photon with respect to its parent lepton, $Q^2 = -q^2 = -(p_e - p_e')^2$, $x = Q^2/2k \cdot q$ and $y = k \cdot q / k \cdot p_e$, α is the fine structure constant and f_γ^e is either the equivalent photon density in the Weizsäcker-Williams (WW) approximation or a beamstrahlung photon density. The $F_k^\gamma(x, Q^2, m^2)$, $k = 2, L$ are the deep-inelastic structure functions for this process. These structure functions receive contributions from both hadronic and pointlike photons, i.e. $F_k^\gamma(m^2) = F_k^{\gamma,PL}(m^2) + F_k^{\gamma,HAD}(m^2)$, $k = 2, L$. Both components were calculated to NLO in QCD in Ref. [14]. Note that the presence of the heavy quark mass ensures that this separation is, through next-to-leading order, unambiguous. It was demonstrated in Ref. [14] (see also [15]) that both components separate naturally in x, as can be seen in Fig. 21: at this high value of Q^2 for $x < 0.01$ the hadronic component dominates, and for $x > 0.1$ the pointlike one. The former is mainly sensitive to the gluon density in the photon, whereas the latter is calculable in perturbative QCD, its only uncertainties stemming from α_s and the charm quark mass.

The high energy and large luminosity of the NLC will lead to a large sample of the single-tag two-photon events containing heavy quarks (mainly charm), making a study of the reaction (35) and its just outlined characteristics very worthwhile.

In Table 4 we give estimates for event rates both for charm and bottom production at the NLC. We show separately the number of events due to beamstrahlung (we again used the TESLA spectrum) and Weizsäcker-Williams bremsstrahlung (we used the expression in Ref. [6] with an "optimistic" anti-tag angle of $\theta_{max} = 40$ mrad) contributions. The numbers are based on the NLO calculation. See Ref. [15] for the parameter choices that went into producing this table and the next. We have summed the contributions due to pointlike and hadronic photons for each entry. For the largest two x bins the contribution of the hadronic component is below 10%, whereas in the two smallest x-bins it is more than 90%. Note that the number of charmed events is truly large, even at large Q^2. The number of events containing bottom quarks is again much smaller due to charge (factor 16) and phase space suppression.

To test the sensitivity to the gluon density, we give in Table 5 the production rate in a small x bin for various choices of parton densities, charm quark mass values and mass factorization scales. Examining the composition of these results, one finds very little contribution due to the hadronic channel from beamstrahlung photons (about 1-2%). Further one finds that the contributions due to pointlike photons both of WW and beamstrahlung origin is similarly small. The numbers therefore indicate that there is a good possibility of measuring the gluon density in the photon using charm quarks at the

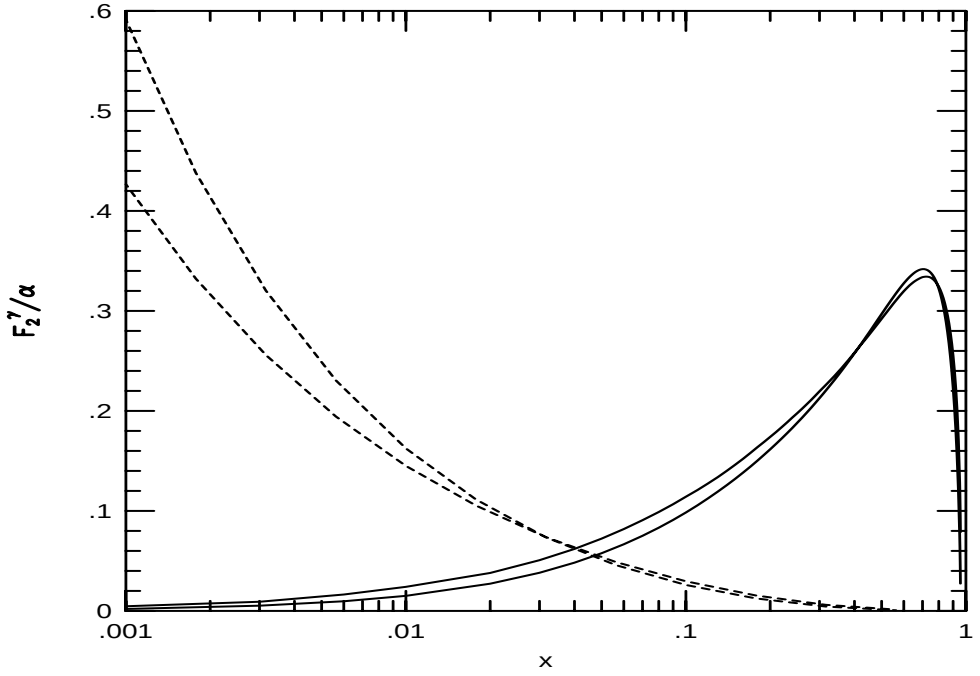

Figure 21: Hadronic (dashed lines) and pointlike (solid lines) components of F_2^γ/α vs. x at $Q^2 = 200\,(GeV/c)^2$. The lower solid line is the leading order (LO), the upper one the next-to-leading order case. The lower dashed line at $x = 0.001$ is the NLO order, the upper one the LO case.

NLC, low charm acceptance notwithstanding. The most significant uncertainty is related to the charm quark mass, however a differentiation of the gluon densities of GRV [5] and ACFGP [16] seems certainly feasible at the NLC.

Bottom quark production is so much more suppressed that a measurement of the photonic gluon density from bottom production in $e\gamma$ scattering at the NLC seems impossible.

For more details and for charm quark kinematic distributions, see Ref. [15].

8.3 Quarkonia production in $\gamma\gamma$ collisions

The radiative decay width of the charmonium states η_c, χ_{c0} and χ_{c2} can directly be measured in two-photon collisions at the NLC. These $\gamma\gamma$ partial widths provide an important test of the non-relativistic quarkonium model (see e.g. Ref. [17] for theoretical details). Accurate analyses of the charmonium states can already be expected at LEP2 [1], while there is little prospect of studying $\gamma\gamma$ production of bottomonium states.

Two-photon production of J/ψ bound states is an attractive tool to determine the gluon distribution in the photon [18]. In contrast to the case of open heavy flavour production, J/ψ mesons are generated predominantly via resolved photons and can be tagged in the leptonic decay modes. The cross section for inelastic J/ψ production in $\gamma\gamma$ collisions at a 500 GeV NLC via the leading colour-singlet channel is predicted to be

~ 50 pb, including NLO corrections [19] and using a coherent superposition of WW and beamstrahlung photons (TESLA design). The cross section appears to be quite sensitive to the parametrization of the gluon density in the photon [20], but clearly more detailed studies including realistic cuts are needed. So-called colour-octet processes, in which the heavy-quark antiquark pair is produced at short distances in a colour-octet state and subsequently evolves non-perturbatively into a physical J/ψ, should contribute to the cross section at some level [21]. The importance of such processes towards a successful description of heavy quarkonia production at the Fermilab Tevatron has recently been investigated in a series of papers [22]. However, their phenomenological significance for J/ψ production has so far not been conclusively established (see Refs. [23] for analyses of colour-octet contributions to J/ψ photoproduction). A measurement of inelastic J/ψ production in $\gamma\gamma$ collisions at the NLC will not only provide information on the gluon distribution of the photon but appears to be a clean test for the underlying picture of quarkonium production as developed so far in the perturbative QCD sector.

Acknowledgements

R.M.G. wishes to acknowledge support from C.S.I.R. (India) under grant no. 03(0745)/94/EMR-II.

References

[1] P. Aurenche et al., $\gamma\gamma$ *Physics*, in: Proceedings of the Workshop *Physics with LEP2*, CERN Yellow report, CERN 96-01, G. Altarelli, T. Sjöstrand, F. Zwirner eds.

[2] M. Drees, M. Krämer, J. Zunft and P.M. Zerwas, Phys. Lett. **B306** (1993) 371.

[3] M. Drees and R.M. Godbole, in: Proceedings of the *Workshop on Physics and Experiments with Linear e^+e^- Colliders*, Waikaloa, Hawaii, April 1993, eds. F.A. Harris et al.

[4] O.J.P. Eboli, M.C. Gonzalez-Garcia, F. Halzen and S.F. Novaes, Phys. Rev. **D47** (1993) 1889

[5] M. Glück, E. Reya and A. Vogt, Phys. Rev. **D46** (1992) 1973.

[6] S. Frixione, M. Mangano, P. Nason and G. Ridolfi, Phys. Lett. **B319** (1993) 339.

[7] P. Chen, T. Barklow and M.E. Peskin, Phys. Rev. **D49** (1994) 3209.

[8] D. Schulte, private communication.

[9] M. Krämer and E. Laenen, CERN preprint CERN-TH/95-291 (hep-ph/9511358), to be published in Phys. Lett. B.

[10] B. Harris, M. Krämer and E. Laenen, in preparation.

[11] M. Cacciari, M. Greco, B. Kniehl, M. Krämer, G. Kramer and M. Spira, DESY preprint DESY 95-205 (hep-ph/9512246), to be published in Nucl. Phys. B.

[12] B. Mele and P. Nason, Nucl. Phys. **B361** (1991) 626; M. Cacciari and M. Greco, Nucl. Phys. **B421** (1994) 530.

[13] M. Cacciari and M. Greco, Z. Phys. **C69** (1996) 459; B. Kniehl, M. Krämer, G. Kramer and M. Spira, Phys. Lett. **B356** (1995) 539.

[14] E. Laenen, S. Riemersma, J. Smith and W.L. van Neerven, Phys. Rev. **D49** (1994) 5753.

[15] E. Laenen and S. Riemersma, preprint CERN-TH/95-324, DESY 95-240 (hep-ph/9602258), to be published in Phys. Lett. B.

[16] P. Aurenche, P. Chiapetta, M. Fontannaz, J.P. Guillet and E. Pilon, Z. Phys. **C56** (1992) 589; P. Aurenche, J.P. Guillet and M. Fontannaz, Z. Phys. **C64** (1994) 621.

[17] G.A. Schuler, CERN preprint CERN-TH.7170/94 (hep-ph/9403387), to be published in Phys. Rep.

[18] M. Drees and R.M. Godbole, Nucl. Phys. **B339** (1990) 355 and Z. Phys. **C59** (1993) 591.

[19] M. Krämer, J. Zunft, J. Steegborn and P.M. Zerwas, Phys. Lett. **B348** (1995) 657; M. Krämer, Nucl. Phys. **B459** (1996) 3.

[20] M. Drees and R.M. Godbole, J. Phys. G, Nucl. Part. Phys. **21** (1995) 1559.

[21] G.T. Bodwin, E. Braaten and G.P. Lepage, Phys. Rev. **D51** (1995) 1125.

[22] M. Cacciari and M. Greco, Phys. Rev. Lett. 73 (1994) 1586; E. Braaten, M.A. Doncheski, S. Fleming and M.L. Mangano, Phys. Lett. **B333** (1994) 548; D.P. Roy and K. Sridhar, Phys. Lett. **B339** (1994) 141; E. Braaten and S. Fleming, Phys. Rev. Lett. 74 (1995) 3327; M. Cacciari, M. Greco, M.L. Mangano and A. Petrelli, Phys. Lett. **B356** (1995) 560; P. Cho and A.K. Leibovich, Phys. Rev. **D53** (1996) 150 and CALT-68-2026 (hep-ph/9511315).

[23] M. Cacciari and M. Krämer, DESY preprint DESY 96-005 (hep-ph/9601276); J. Amundson, S. Fleming and I. Maksymyk, MADPH-95-914 (hep-ph/9601298); P. Ko, J. Lee and H.S. Song, SNUTP-95-116 (hep-ph/9602223).

σ [nb]	$m_c = 1.3$ GeV $\mu = m_c$	$m_c = 1.5$ GeV $\mu = \sqrt{2}\, m_c$	$m_c = 1.7$ GeV $\mu = 2m_c$
direct	6.88	5.68	4.78
1–res	6.69	3.72	2.92
2–res	0.21	0.12	0.07
total	13.8	9.52	7.77

Table 3: Total cross sections for $e^+e^- \to e^+e^- + c\bar{c}X$ at $\sqrt{s} = 500$ GeV. Input parameters as described in the text.

Q^2	x	Events			
range	range	c(WW)	b(WW)	c(Beam)	b(Beam)
100 - 320	$1.0 - 3.2 \cdot 10^{-3}$	1040	80	0	0
	$3.2 - 10.0 \cdot 10^{-3}$	3790	300	220	20
	$1.0 - 3.2 \cdot 10^{-2}$	6230	430	3150	200
	$3.2 - 10.0 \cdot 10^{-2}$	10,300	510	12,200	580
	$1.0 - 3.2 \cdot 10^{-1}$	21,700	830	34,700	1320
	$3.2 - 10.0 \cdot 10^{-1}$	43,300	730	73,800	1240
320 - 1000	$1.0 - 3.2 \cdot 10^{-2}$	1050	110	70	10
	$3.2 - 10.0 \cdot 10^{-2}$	2310	160	1230	80
	$1.0 - 3.2 \cdot 10^{-1}$	5610	260	6790	310
	$3.2 - 10.0 \cdot 10^{-1}$	13,300	400	21,200	620

Table 4: Event rates of $e\gamma$ collisions producing charm and bottom quarks at the NLC with a luminosity of 20 fb^{-1} and $\sqrt{S} = 500$ GeV.

Charm Mass	Q^2 range	x range	Events		
			$\mu_f = Q/2$	$\mu_f = Q$	$\mu_f = 2Q$
1.3	32 - 100	$1.0 - 3.2 \cdot 10^{-3}$	2080	2140	2230
1.5			1880	1890	1930
1.7			1740	1750	1790
1.3	100 - 320	$1.0 - 3.2 \cdot 10^{-3}$	346	356	370
1.5			987	1024	1058
1.7			907	930	954
1.3	32 - 100	$1.0 - 3.2 \cdot 10^{-3}$	3770	4080	4500
1.5			3490	3740	4090
1.7			3240	3480	3810
1.3	100 - 320	$1.0 - 3.2 \cdot 10^{-3}$	478	509	561
1.5			774	854	943
1.7			716	777	847

Table 5: Event rates at small x at the NLC with a luminosity of 20 fb^{-1} and $\sqrt{S} = 500$ GeV. We used GRV [5] parton distributions in the $\overline{MS}$ scheme for the top half and ACFGP [16] for the bottom.